DESIGN AND DEVELOPMENT OF HIGH SHEAR MIXER

A DISSERTATION

Submitted in the partial fulfillment of the
requirement for the award of the degree

Of

MASTER OF TECHNOLOGY

In

CHEMICAL ENGINEERING

(With Specialization in Computer Aided Process Plant Design)

By

VIKASH

DEPARTMENT OF CHEMICAL ENGINEERING

INDIAN INSTITUTE OF TECHNOLOGY

ROORKEE- 247667 (INDIA)

JUNE, 2013

DECLARATION

I hereby assure that the work presented in this dissertation report entitled **"Design and Development of High Shear Mixer**" is submitted towards completion of dissertation work in M.Tech (CAPPD) at the Indian Institute of Technology Roorkee, is an authentic record of my original work carried out under the guidance of **Dr. Vimal Kumar**, Assistant Professor. I have not submitted the matter embodied in this dissertation report for the award of any other degree.

Place: Roorkee **Vikash**

Date:

CERTIFICATE

This is to certify that Mr. Vikash has completed the dissertation report entitled "**Design and Development of High Shear Mixer"** under my supervision. This is to certify that the above statement made by the candidate is correct to the best of my knowledge.

Dr. Vimal Kumar

Assistant Professor,

Department of Chemical Engineering

Indian Institute of Technology, Roorkee

ACKNOWLEDGEMENT

I am greatly indebted to my guide **Dr. Vimal Kumar**, Department of Chemical Engineering, Indian Institute of Technology Roorkee, Roorkee for his kind support and guidance during the entire course of this work. His cooperation and in depth knowledge have made my work possible.

I am also thankful to **Dr. V.K. AGARWAL Prof and Head**, Department of Chemical Engineering and other staff members for their instant help in all kinds of work. I would like to thank my friends for their continuous support and enthusiastic help. Last but not least, it is owed to the blessings of my parents and God that I have come up with this work in due time.

Vikash

ABSTRACT

High shear mixers (HSMs), characterized by their highly localized energy dissipation, and are widely used in process industries for dispersed phase size reduction and reactive mixing. In order to create the highly localized energy dissipation a rotor stator assembly is required, also known as rotor-stator mixer (RSM). In this report various research articles on high shear mixers are reviewed. These include the application and uses of high shear mixers, their geometry, and their hydrodynamic characterization using computational fluid dynamic (CFD) techniques.

Power draw is a characteristic parameter to describe the dynamic mixing state, which is fundamental to motor selection in the mixer design, optimization and scale-up. Therefore in the present work the CFD modeling of an existing HSM and a proposed novel HSM design is carried out using k-ε turbulence model. The results in both existing and proposed design are reported in terms of power draw, flow patterns and energy dissipation. The simulations were carried out using transient sliding mesh with k-ε turbulence model at a rotor speed of 4000 rpm for the validation with the existing results. The existing HSM is comprised of square holes in the stator and a rotor with 4 blades. The proposed mixer design is comprised of tilted jets/holes in the stator, for the deep penetration in the mixing vessel. For the optimization of operating as well as geometrical parameter of the proposed mixer design, the simulations are carried out at different rotor speeds. The mixing characterization of the square holes and proposed high shear mixer are also studied in this present work.

CONTENTS

LIST OF TABLES

LIST OF FIGURES

NOMENCLATURE

D	Rotor diameter (m)
H	Tank height
M	Mass flowrate (kg/s)
N	Rotor speed (1/s)
P	Power (W)
P_0	Power number (P/N^3D^5)
P_T	Power due to torque (W)
r	Radial direction (mm)
Re	Reynolds number (rnd^2/μ)
S_{ij}	Strain rate based on time averaged velocity (m/s^2)
t	Time (s)
T	Tank diameter
U_{rad}	Radial velocity (m/s)
U_{tan}	Tangential velocity (m/s)
Z	Axial coordinate (mm)
u_i	Instantaneous velocity in i direction (m/s)
U_i	Time or ensemble average velocity in i direction (m/s)
$u\tau$	Friction velocity (m/s)
u_i'	Fluctuating component in i direction (m/s)
α	Hole orientation (^{o})
β	The angle between the leading and trailing edges (^{o})
δ	Gap spacing (m)
ϵ	Turbulent energy dissipation rate per unit mass (m2/s3)
γ	The angle between jet shear layer and tangent at trailing edge (^{o})
φ	Blade position relative to q = 0 (^{o})
θ	Tangential coordinate (^{o})
ρ	Density (kg/m^3)

CHAPTER 1

INTRODUCTION

1.1 High shear mixers

A high-shear mixer is a device which disperses one phase (liquid, solid, gas) into a main continuous phase (liquid), with which it would normally not be miscible. This requires high and intense rate of mixing hence a rotor or impellor, together with a component that is known as a stator, or many rotors and stators together forming a group, is used either in a tank containing the solution that is to be mixed, or in a pipeline through which the solution passes, to invoke intense lateral mixing of the two phases which results in shear hence the name high shear mixers. The principle of high shear mixing is of great use and hence used in many industrial applications to produce emulsions, suspensions, adhesives and also granular products.

1.2 Principle of operation

Fluid is said to experience shear when one part of fluid travels with a varied velocity relative to a nearby part of the fluid. A high-shear mixer requires a rotor and a stator like Couette Rotor–Stator, as shown in Fig.1.1. As the name implies one part is a high-speed rotor or a group of such parts or continuous rotors forming a series, attached to an electric motor, for fluid mixing, creating flow and shear. The speed of the fluid at the outer diameter of the rotor is higher than the speed at the center (inside) of the rotor, and this velocity difference between the inside and outside fluid creates shear.

The other part is an immovable component attached with the rotor, and is called stator. The stator provides a gap with a low spacing between the rotor and itself. The rotor exit fluid has a very high shear rate. The rotor and stator together is used as the generator. More the generators more will be the shear. The important design configurations of a high shear mixture are given as:

1. Rotor diameter and speed.
2. The gap between the rotor and the stator.
3. The time in the tank, and the number of generators in the series.

4. Variables range from the count of rows of teeth, their angle, and therefore the dimension of the openings between teeth.

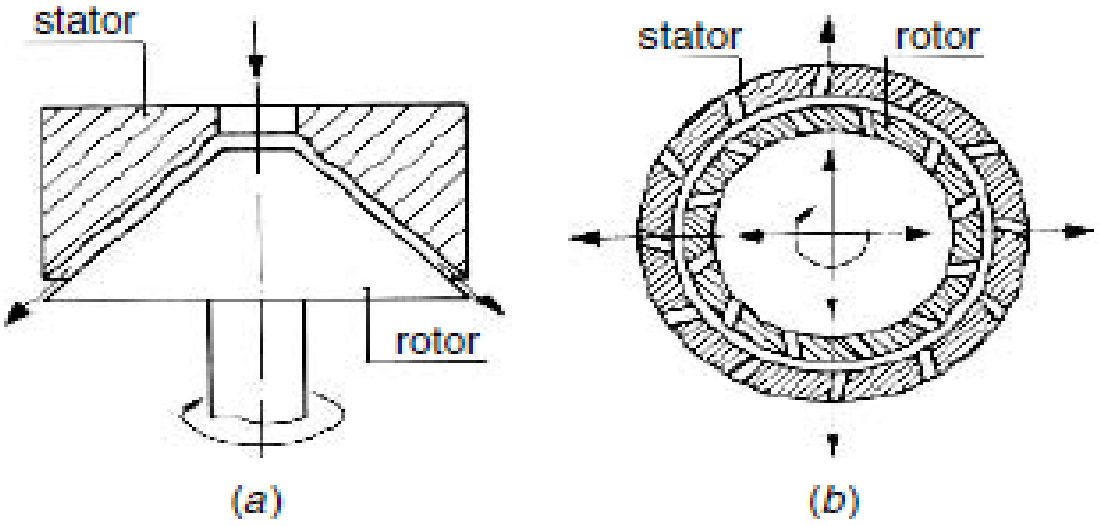

Fig. 1.1 Couette Rotor–Stator geometry, (a) Simple Couette; (b) Toothed rotor–stator (Source: Handbook of industrial mixing science and practice)

High shear mixers are widely used in almost all chemical industries as they have wide applications ranging from simple single or multi- phase blending to complex multi-phase reaction systems. There are various companies which are engaged in manufacturing high shear mixers but the major market is captured by **Silversons** which supply a range of high shear mixers from simple to the most complicated ones. Other companies dealing with the production of these are **Ross high shear mixers etc.** The main objective of the present work is the mixer design for the better mechanical agitation and to study the hydrodynamics and mixing behavior for the proposed novel mixer. The commercial computational fluid dynamics (CFD) softwares are often used to simulate of varied flow, e.g. in mechanically stirred vessels. The operating efficiency and design parameters can be improved by this approach. The mixer geometry is developed and optimized using CFD software, ANSYS.

Following three models would be studied for this purpose:

1. Reynolds Stress Model (RSM)
2. The k–ε turbulence model would be considered for further study

3. Large Eddy Simulation(LES)

The k–ε turbulence model would be helpful to predict the hydrodynamic characteristics of viscous fluid flow and power draw in a high shear mixer, which is an important consideration for the use of rotor stator mixer in industries.

1.3 Motivation and objectives

High shear mixers have wide application and scope in process industries therfore the study and research of design and development is highly beneficial. Although an ample amount of research has been done in this area but still a lot remains to be understood. There are different parametrs which are not well stuided like, mixing in a rotor-stator assembly and there geometry effects on performance. In the present work it is proposed to carry out detailed literature review and design and development of a high shear mixer for viscous fluids. Apart from detail literature review of high shear mixers, the objectives of the present work are as follows:

- State of the art review for the high shear mixers.
- Model development and grid topology in rotor-stator high shear mixer with square hole stator.
- Methodology validation and comparison with the existing results available in the literature.
- To investigate the flow pattern, energy dissipation and power draw in square stator high shear mixer.
- On the basis of the previous results, optimization of the proposed mixer design.
- To study the mixing charactristics in the proposed novel model and square holes rotor-stator model.

CHAPTER 2

LITERATURE

Ample amount of research has been carried on high shear mixers, power consumption expression, their geometry, residence time distribution and mixing times. The literature available on these parameters has been studied and reviewed. Besides this research papers that highlighted the application of these in various industries are also reviewed. There are various known specifications and divisions of high shear mixers based on their speed and mode of operation. On the basis of mode of operation these are categorized into two:

1. Batch High Shear Mixer
2. In-line High Shear Mixer

2.1 Batch high-shear mixers

In a batch high-shear mixer, the fluids are fed from the top and a rotating shaft containing the mixer is present at the bottom of the tank. A batch high-shear mixer is shown in Fig. 2.1. In batch high shear mixers a given volume of material can be mixed approximately twice faster than an inline rotor–stator mixer with the same power rate; Such mixers are used in the area of where space is limited and fast processing is required. However cleaning is required for the mixing of sticky solutions. There are configurations of such high-shear mixers that have a part of the operating run to clean the tank. To limit the cleaning some dry run high-shear mixers are also designed.

2.2 In-line high-shear mixers

An inline high-shear rotor–stator mixer has an inlet at one side and an outlet at the other end and the rotor rotate through a seal. The components are mixed through the generator array in a continuous stream manner, and behave like centrifugal pumping device. Inline high-shear mixers as given as in Fig. 2.2 having a more stable mixing environment, less requirement of space, and

used as a continuous process. For achieving the equilibrium mixing, the product must be passed through the mixer more than once.

Fig. 2.1 A batch high shear mixer (Source: Silversons)

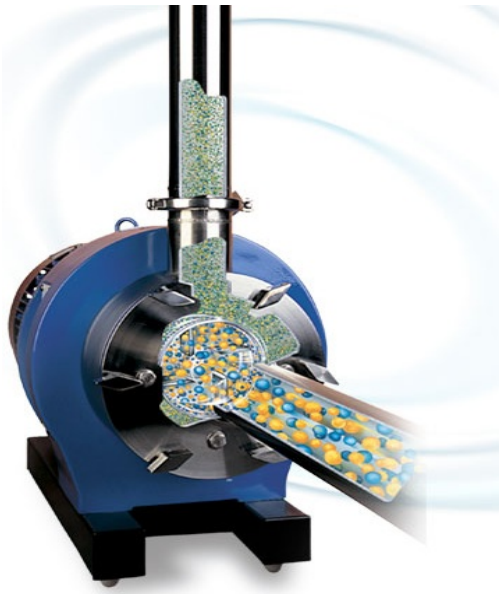

Fig. 2.2 An inline high shear mixer (Source: Silversons)

These are the main types of high shear mixers however the company Silversons is reported to manufacture several modified versions of these mixture for various industrial applications like laboratory mixer, laboratory in-line mixer, ultra-mix mixer, in-line ultra-sanitary mixer etc. and these can be seen in Fig. 2.3. There are various Geometrical descriptions of commercial high shear mixers used in chemical industries:

2.3 Rotor-Stator mixers- a high shear mixer

A rotor/stator mixer, also termed as high shear mixer, generally comprises of a four-blade rotor rotating at a high tip speeds within a close tolerance stator, typically in the range of 2,000 to 8,000 rpm. High levels of mechanical and hydraulic shear are applied in the mixer and stator zone similar to high shear mixers. Ultra-high shear mixer designs with rotors run up to 30,000 rpm have been widely used in energy intensive processes such as dispersion, emulsification,

grinding, dissolving, and cell disruption in the fields of agricultural land food production and chemical reaction processes etc.

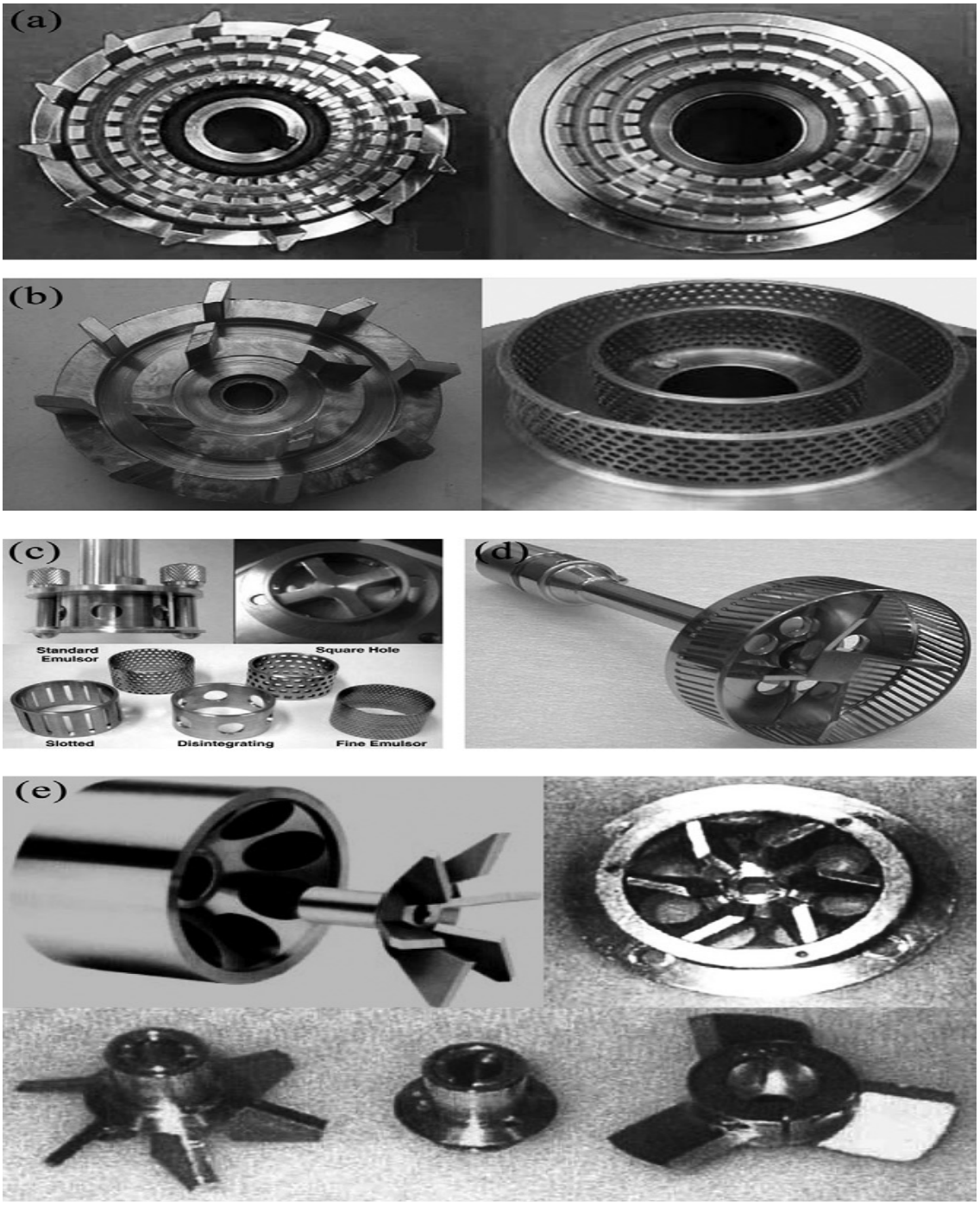

Fig. 2.3 Geometric descriptions of commercial high shear mixers (Source: Zhang et al, 2012)

Solomon et al, (1981) considered an idealized spherical cavern centered on the impeller (Rushton turbine) and proposed a generalized model based on torque balance; their model assumes that the flow within the cavern is tangential. By using the viscous Newtonian fluids in the laminar regime, the hydrodynamics characterization of a rotor-stator assembly has been carried out by Barailler (2006).

The finite element numerical methodology has been used to model the velocity patterns, the flow rate and shear stress distribution through the head. VFEM feature of POLY3D^{TM} (Rheosoft) was used to for the CFD simulations.

It has been found that there was a good agreement of numerical prediction of the power consumption and also with the flow profiles. The effects of Reynolds number and speed limit on the generation of a pseudo-cavern were also studied. The similar experimental setup was used as used by the Doucet et al, (2005).

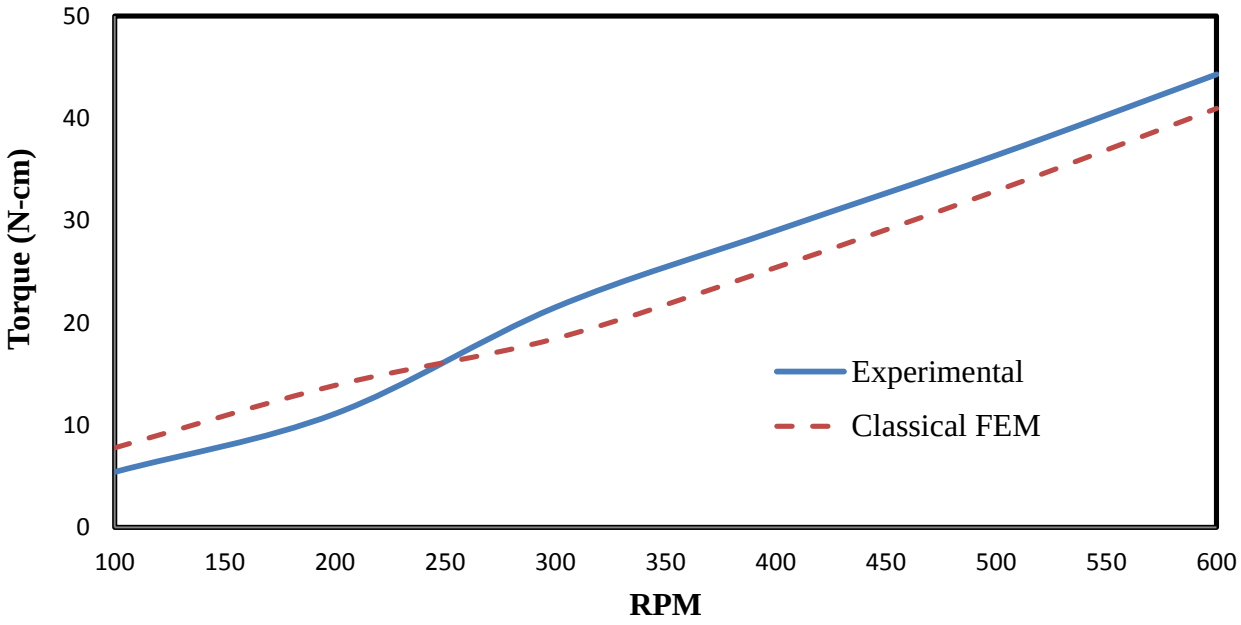

Fig. 2.4 Experimental and numerical Torque versus RPM (Source: Solomon et al, 1981)

The simulated predictions of Solomon et al, 1981 were in good agreement with their experimental results, as shown in Fig. 2.4.

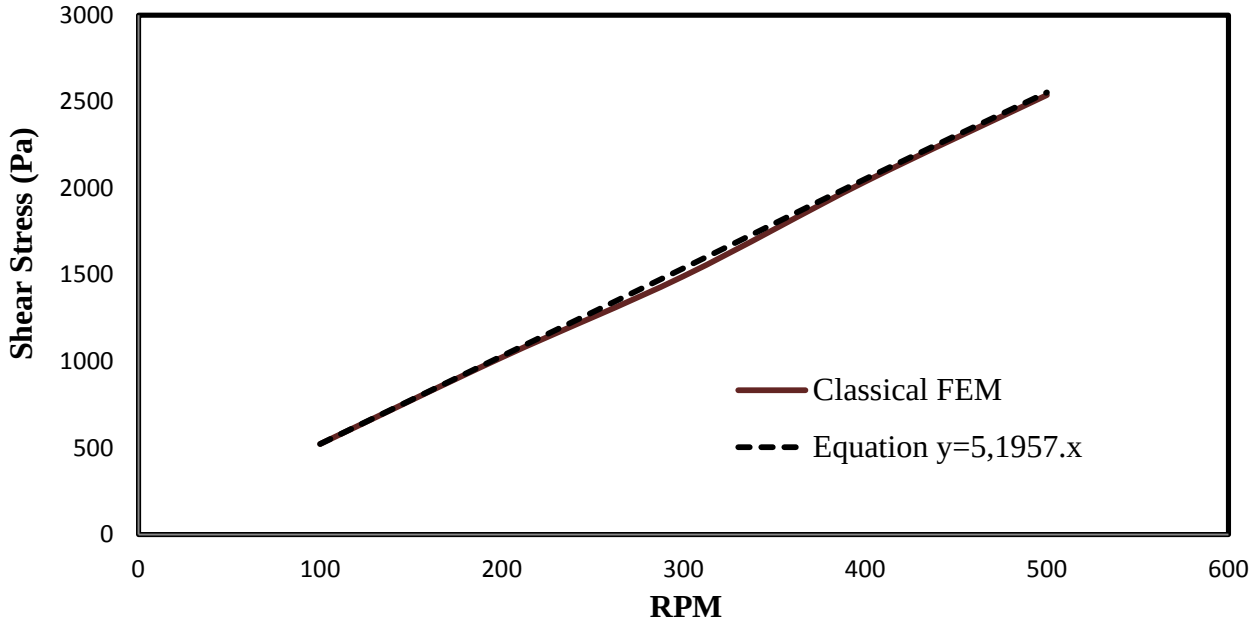

Fig. 2.5 Maximum shear stress versus RPM (Source: Solomon et al, 1981)

According to them the simulated data showed that there is a high stress in the gap between rotor and stator. In the Fig. 2.5 it is shown that the pseudo-cavern size scales with the classical definition of the Reynolds number and fits with the pseudo-cavern obtained by tracking the trajectories of massless particles.

Calabrese et al, (2002) simulated the inline rotor-stator assembly. The slotted head stator was used and the $k-\varepsilon$ turbulence model has been used to simulate. The used model has been a 2D sliding mesh and the basic RANS equation was solved. It has been shown that there is no effect of mechanical forces on the emulsification for the lower value of Reynolds number i.e. Re=104. It has also been studied that there is no dispersion effect at this low Reynolds number as if there is any mechanical forces generate in the gap. The mixing increased due the high flow in the jets and there must be a swirl in the tank near the rotor-stator head. **Thakur et al, (2002)** studied a 3D model instead of 2D. The simulation was performed using the finite volume method and $k-\varepsilon$ turbulence model. They used a quasi-steady rotor-stator in a centrifugal blower. Simulated results and experimental results were in good agreement in there studied. They predicted the rise of static pressure. The simulated results of power consumption and flow rate were in good agreement.

Doucet et al, (2005) characterized hydrodynamics in a high shear rotor-stator mixer in terms of power draw and flow patterns with viscous Newtonian and shear thinning fluids. The power consumption was correlated which determined the pseudo-cavern dimension as a function of hydrodynamics parameters. It was observed that the impeller shear rate constant, was found to be dependent on the fluid rheological properties. It has been reported that the shape and magnitude of the pseudo-caverns in the vicinity of the rotor-stator mixer are required to understand the relationship between the power draw and the ability of the impeller to mix the fluid into the vessel. Glucose solutions were used as Newtonian fluids and Xanthan gum (KeltrolRD, CP Kelco) and sodium carboxymethyl cellulose (grade 30000, Cekol—thereafter called CMC) solutions were used as non-Newtonian fluids. The rotor-stator impeller used is shown in the Fig. 2.6.

Fig. 2.6 Image of a Rotor-stator impeller (Source: Barailler et al, 2006)

Doucetet al, (2005) predicted caverns size and power consumption during a conversion process in order to control the overall mixing in a tank. Several regimes were described and allow the designer to predict the approximate cavern shape when performing scale-up. A flow visualization technique based on a fast acid/base reaction described by **Brennan et al, (1976)** and also by **Arratia et al, (2004)** to characterize the cavern shapes of Newtonian fluids. It was observed that effects of Reynolds number on the shape of cavern. The shape of a right circular cylinder was observed for the low Reynolds number. The lower part of the tank i.e. mixed part was grow faster as compared to the upper part as the Reynolds number increased from there

lower value to the high value. The pseudo-cavern has a kind of pine tree shape as shown in Fig. 2.7.

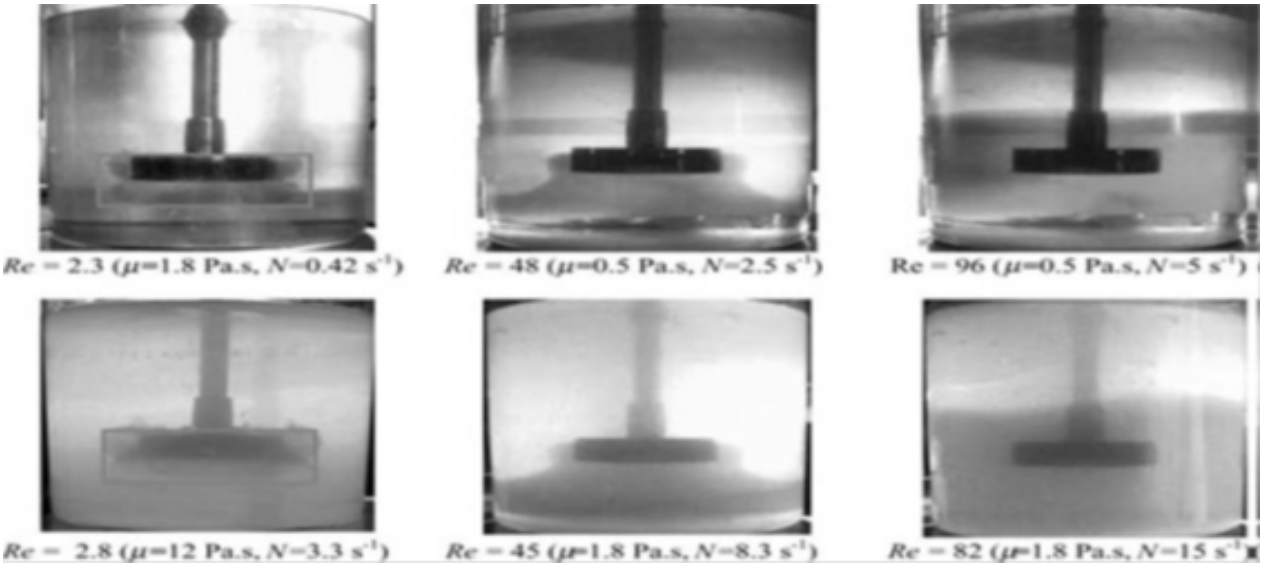

Fig. 2.7 Evolution of cavern shapes of Newtonian fluids (Source: Doucet et al, 2005)

They also observed a different pseudo-cavern phenomenon with non- Newtonian fluids and reported that at the same Reynolds number, the pseudo-cavern size and shape is influenced by the apparent viscosity near the impeller as shown in Fig. 2.8. It can be seen that the cavern size and shape do scale with the Reynolds number. Pseudo-caverns observed in Newtonian fluids scale with respect to the Reynolds number while in case of non-Newtonian fluids scale with Re_y (ratio of the inertial forces due to the fluid motion to the fluid yield stress).Therefore In order to control the mixing process it is required to predict cavern size and power consumption during a conversion process.

Pacek et al, (2007) simulated the fluid flow in a rotor-stator mixer. They used the sliding mesh method and standard *k-ε* turbulence models at different rotor speeds and verified them using LDA. The flow rate through stator holes was directly proportional to the speed of rotor. The edge of the stator holes contained a stagnation point where a maximum rate of energy dissipation was reported. The experimental measurements were in good agreement however there was a under prediction of maximum jet velocity emerging from stator holes. It has been reported that the numerically simulated flow number was lower than those obtained from LDA measurements. It was also observed the LDA measurements based on energy balance which indicated a 70% of

the energy dissipation in the mixer head. Although the k-ε model predicted energy dissipation in the different region of the rotor stator assembly but the energy dissipation for rotor swept volume, gap between rotor and stator, walls of the holes and the jets were 50%, 5%, 8% and 16%, respectively.

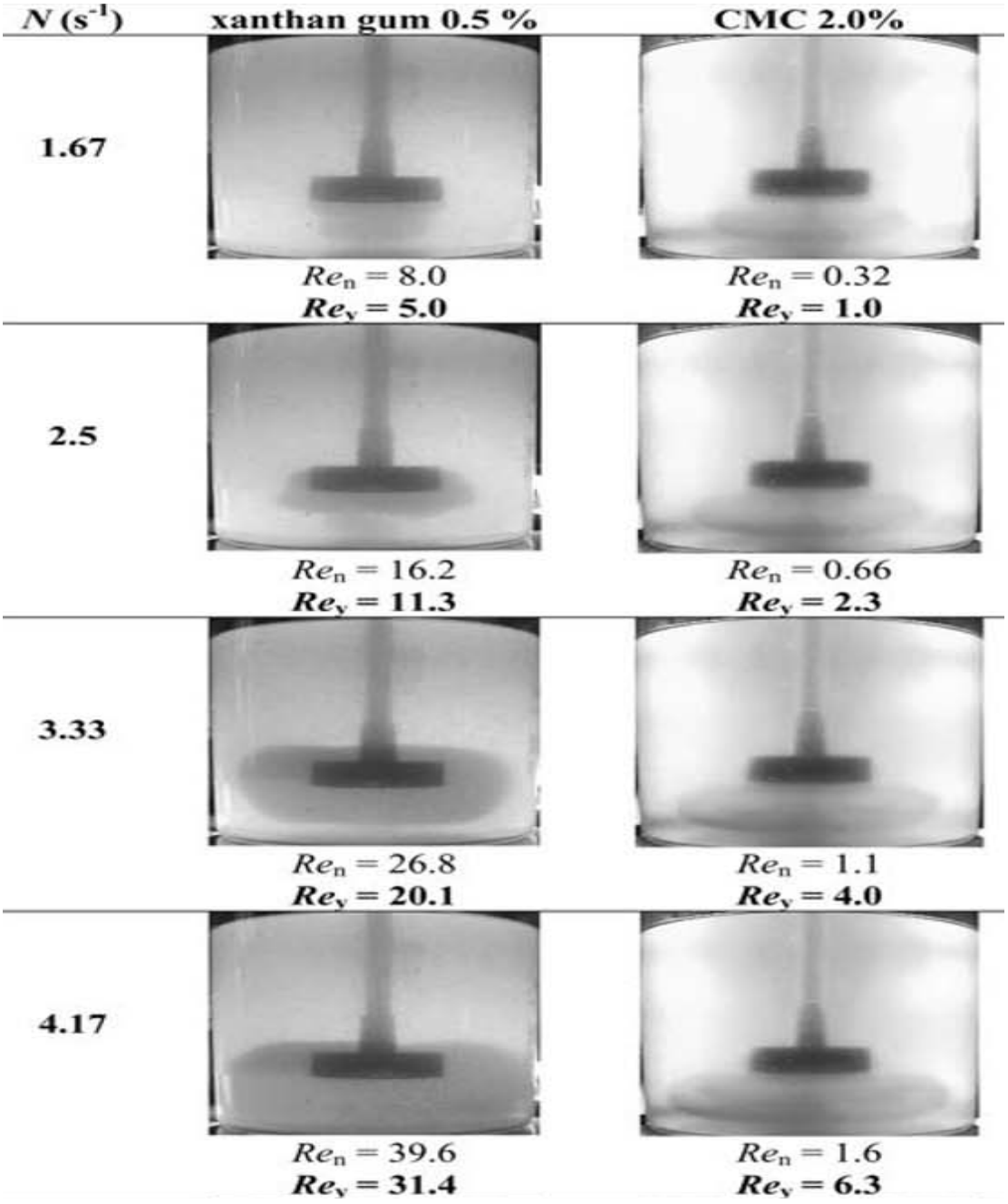

Fig. 2.8 Evolution of cavern shapes with non- Newtonian fluids (Source: Doucet et al, 2005)

Utomo et al, (2009) studied the effect of stator geometry on the rate of energy dissipation and flow pattern in a rotor–stator assembly. The different rotor-stator geometry is shown in the Fig. 2.9. To study the effect of geometry they used the standard *k*– *ε* turbulence model. It has been reported that the liquid and rotor rotates in the counter direction as compared to each other at the certain distance and the stators contained the narrow openings and this flow was produced because jets having a strong circulation flows behind. There was a good agreement of power numbers for these different geometries with the experimental results. For square and disintegrated holes stator the predicted power numbers are as low to 10% as compared to experimental results but 20% for the slotted head stator.

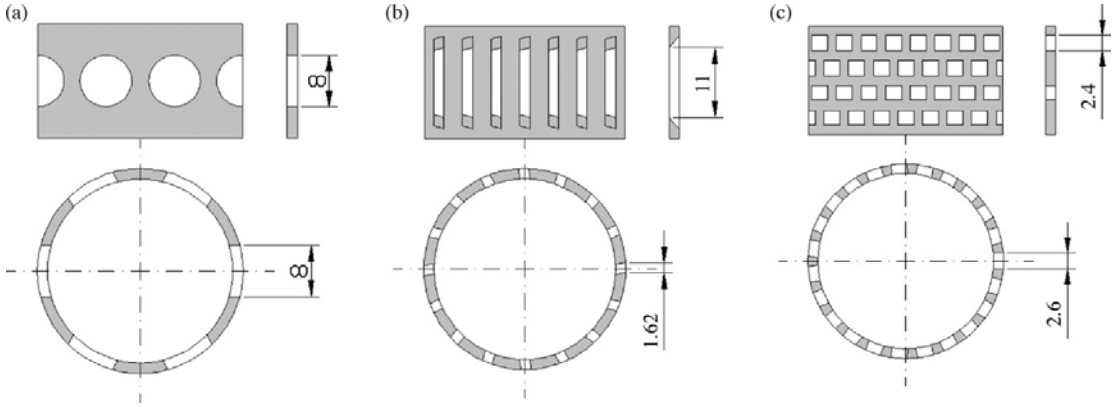

Fig. 2.9 Stator geometries investigated in this work: (a) disintegrating head, (b) slotted head and (c) square hole head (Source: Utomo et al, 2009)

With the help of experimental as well as numerical studies it has been demonstrated that the flow patterns were same for all the geometries and there were no effect of size of holes on the flow pattern. There was a circulation pattern of the fluid as the jets exist from the holes and the pattern is behind the jets. According to their study the rate of energy dissipation increases as the size of the holes decreases. The small size holes created the more uniform energy dissipation rate because there is a uniform drop size distribution (DSD) for the small holes and they created the uniform dissipation of energy. It was reported that the power number changed according to change in the flow rate but flow rate changed according to total holes area. **Kowalski et al, (2011)** reported the validation of an expression to accurately describe the power draw of an in-line rotor–stator mixer over a range of flow rates and rotor speeds.

Viazzo et al, (2012) predicted the turbulence flow by quantitative comparisons of two high-order LES methods in rotor-stator mixer. The spectral vanishing viscosity technique and dynamic Smagorinsky (1963) (classical model) the SGS stress model were compared. The mean velocity, time dependent flow structures and components of Reynolds stress tensor were described by using both LES methods. A spectral SVV approach has an advantage of accuracy and cost of CPU. They also reported that LES results are improved over the RANS results for fully developed turbulent and transition flow.

Recently **Zhang et al, (2012)** reviewed typical applications of high shear mixers. Practical applications of HSMs can be classified into three typical categories:

1. Liquid–liquid emulsification, to produce less viscous liquid–liquid dispersions, highly viscous emulsions like mayonnaise and bitumen, and mini-emulsions with controlled droplet sizes for desirable polymerization etc.
2. Solid–liquid suspension, for the medicine, electronic and healthcare products to produce uniform nanoparticles suspensions; to produce micronized waxes dispersions used in ink, and coatings and the pigment or dye-based solid inks; to handle the wet milling of active pharmaceutical ingredients (APIs); in recovery processes of fermentation to disrupt cells, and even to control over the crystallization of pharmaceutical products.
3. Chemical reactions, to produce fine chemicals or intermediates, e.g. the production of linear alkyl-benzenes, chloro-benzene, toluene, di-isocyanate, toluene-diamine and aniline and polymers like lastisols and fluidized bed coating that are made by suspension polymerization,

Many industries make products or provide services that are connected with fluid flow and associated multiphase (gas, liquid and solid particles) processes, which are fundamental to national economy in all countries because they are central to all major process industries - energy, minerals mining, chemical industries, pharmaceuticals production, food and metallurgical processing. Throughout industry, fluid solid two-phase flow unit operations are one of the most troublesome to operate. The flow behavior of these two-phase systems is too complex in order to reliably scale-up, design or optimize them. Typically, experimental testing is performed on expensive, larger-scale units for “effective” new designs or new units mimic present day units.

Recently **Jasińska et al, (2013)** presented a rotor-stator assembly model to predict the power input and also the turbulence structure details. The results of power input and product distributions were confirmed by comparing model predictions data and experimental values. They investigated power measurements and CFD on inline rotor-stator mixer having Silverson double screen size 150/250MS with a diazo coupling of 1 and 2-naphtols and diazotized sulphanilic acid simultaneous multiple reactions. The standard k–ε turbulence model and the multi-reference frame approach were used to simulate the course of chemical reactions, mixing and the hydrodynamics in the rotor-stator mixer.

CHAPTER 3

MODELLING AND SIMULATION

CFD uses advanced computer models and softwares to simulate the fluid flow or multiphase through a processing facility or unit. The application of CFD models and codes by the industry and engineering community has increased considerably in the last few years. This rise in interest and the use of CFD codes is the result of improvements made in the predicting capabilities of CFD models, reductions in the cost of computer hardware, and rise of the costs to perform laboratory experiments and to maintain experimental facilities. The development of reliable CFD models would reduce the need for expensive large-scale test facilities.

3.1. Introduction

The fluid flow, either laminar or turbulent, is governed by continuity and momentum equations. The continuity equation is basically the mass balance and can be written in Eulerian or stationary coordinate as (Versteg and Malalasekera, 1996)

$$\frac{\partial \rho}{\partial t} + \frac{\partial (\rho u_i)}{\partial x_i} = \frac{\partial \rho}{\partial t} + u_i \frac{\partial \rho}{\partial t} + \rho \frac{\partial u}{\partial x_i} \tag{3.1}$$

where ρ is the fluid density and u_i is the instantaneous fluid velocity in x_i direction. For incompressible fluid, eq. 3-1 becomes

$$\frac{\partial u_i}{\partial x_i} = 0 \tag{3.2}$$

In the absence of body forces like centrifugal, gravity, Coriolis and electromagnetic forces, the momentum balance can be written in Lagrangian or moving coordinate as (Davidson, 2004)

$$\frac{D(\rho u)}{Dt} = -\frac{\partial P}{\partial x_i} + \frac{\partial \tau_{ij}}{\partial x_j} \tag{3.3}$$

where $\frac{D(\rho u)}{Dt}$ is the acceleration of the fluid in the control volume , $\frac{\partial P}{\partial x_i}$ is the normal stress due to pressure difference and $\frac{\partial \tau_{ji}}{\partial x_j}$ is the shear stress due to viscous forces. τ_{ji} ndicates shear stress component acting in the j-direction on a surface normal to the i-axis. For Newtonian fluids, shear stress is proportional to the strain rate tensor, and τ_{ji} can be written as

$$\tau_{ij} = 2\mu s_{ij} \tag{3.4}$$

where μ is the viscosity of the fluid and s_{ij} is the strain rate tensor

$$s_{ij} = \frac{1}{2}\left(\frac{\partial u_i}{\partial x_j} + \frac{\partial u_j}{\partial x_i}\right) \tag{3.5}$$

By substituting the shear stress term in eq. 3-3 with eq. 3-4 and eq. 3-5 and assuming that the fluid is incompressible, the momentum balance can be written in Eulerian coordinate as (Davidson, 2004)

$$\frac{\partial u_i}{\partial t} + u_j \frac{\partial u_i}{\partial x_j} = -\frac{1}{\rho}\frac{\partial P}{\partial x_i} + \nu \frac{\partial^2 u_i}{\partial x_j \partial x_j} \tag{3.6}$$

where ν is the kinematic viscosity of the fluid, $\nu = \mu/\rho$. Eq. 3-6 is known as Navier-Stokes equation.

3.2 Solution of the equations

The solution of the momentum balance (eq. 3.3) together with the mass balance (eq. 3.1) depends on the flow geometry and boundary conditions (wall, inlet, outlet, symmetry, etc). However, its analytical solution is almost impossible, except for laminar flow in a very simple geometric, such as pipe, where the flow is practically one dimensional and assumption can be made to simplify the equation. To obtain numerical solution of those equations, the flow domain is divided into many control volumes or computational cells which can be quadrilaterals or triangles in 2D domain or tetrahedral, prisms, pyramids or hexahedra in 3D domain (Marshall and Bakker, 2004). The partial differential equations of mass and momentum balances are discretized into algebraic equations which can be solved numerically. There are various techniques to discretized partial differential equations such as finite volume method (used by commercial CFD packages Fluent, CFX and StarCD), finite element method (used by POLY3D and Comsol), spectral method and lattice Boltzman method (Eggels and Somers, 1996; Derksen, 2001).

In finite volume method, the values of all variables (such as velocity components, pressure and temperature) are stored in the center of computational cells, but they are evaluated at the cell faces. To obtain the values of these variables at cell faces as a function of those at cell centers, a discretization scheme is needed (Marshall and Bakker, 2004).

In this section, the turbulent modeling and the comparison of turbulence models are discussed but the details of discretization schemes and methods of solving the discretized equations are discussed further elsewhere (Patankar, 1980; Versteeg and Malalasekera, 1995; Marshall and Bakker, 2004) and finally, this chapter recommends turbulence model suitable for rotor-stator mixer simulation. Following three models may be used for the simulation of different turbulence.

- Direct numerical simulation (DNS).
- Large eddy simulation (LES).
- Reynolds Averaged Navier-Stokes (RANS) models.

The direct numerical simulation (DNS) is a technique in CFD to solve Navier-Stoke's equations numerically in which there is no turbulence model required for the solution. However, the computational expenses of DNS increases majorly with the Reynolds number and with current capabilities of computing power, it is not practical to do such simulation for a turbulent flow at high Reynolds number typically found in industry or engineering research. In order to overcome the limitation of computational resources, turbulence model is generally used.

In DNS, 99.99 % of computational resources are used to simulate the behavior of small to intermediate scale eddies. About 0.01 % are used to simulate large scale eddies which are behind the transport of momentum, mass, energy, and components are more interesting than small eddies (Davidson, 2004). Large eddy simulation (LES) is an intermediate technique between DNS and RANS. It solves three-dimensional, time dependent continuity and momentum balance equations for large scale eddies and models the effect of small scale eddies. The computational resources required by LES are 10 to 1000 time less than DNS, but 10 to 100 times more than RANS based model.

To overcome the limitation of computational resources, turbulence model is used. One class of turbulence models is Reynolds Averaged Navier-Stokes (RANS) turbulence model. It based on the Reynolds decomposition which divides turbulent flow into 2 components –one is the mean velocity and the other is a fluctuating component.

Velocity component in a point in turbulent flow, u_i, can be written as

$$u_i = U_i + u_i'$$

where *Ui* is the mean velocity component which is the time or ensemble average of u_i and u_i' is the fluctuating component of u_i.

The time or ensemble average of u_i' is zero, but the root mean square of u_i' is not. Generally, the closure model for RANS equation can be divided into eddy viscosity model and shear stress transport model.

3.2.1 Eddy viscosity model

The eddy viscosity concept is based on the Boussinesq approximation which states that Reynolds stresses can be expressed in terms of mean rate of strain of the mean velocity field.

$$\overline{u_i'u_j'} = -\nu_t\left(\frac{\partial U_i}{x_j} + \frac{\partial U_j}{x_i}\right) + \frac{2}{3}k\delta_{ij} \qquad (3.6)$$

where ν_t is the turbulent viscosity, k is the turbulent kinetic energy per unit mass and δ_{ij} is Kronecker delta (δ_{ij} = 1 if i = j, otherwise δ_{ij} = 0).

Based on the number of partial differential equations, the closure model can be a zero-equation (algebraic) model, one-equation model or two-equation model.

The main drawback of one-equation model is the same as zero equation models that is the length-scale must be prescribed algebraically. Therefore the above models are not discussed in this chapter.

3.2.1.1 Two - equation model

The flow turbulence properties can be model by using these models and they contain two extra transport equations. The diffusion and convections turbulent energy effects can be modeled by these models. Following are the two equation models:

(a) *k*-ε model
(b) *k*- ω model
(c) Realisability issues

For the rotating bodies *k*-ε model produces the best results. Other two equation models are not consistent for the rotating bodies. Therefore *k*-ε model is used in the present work. The most popular of two-equation models is *k*-ε turbulence model and therefore only this model is discussed here. In this model, the length scale and turbulent viscosity are expressed in *k* and ε as follows

$$l = \frac{k^{\frac{3}{2}}}{\varepsilon} \qquad (3.7)$$

$$\nu_t = C_\mu \frac{k^2}{\varepsilon} \quad (3.8)$$

The k- ε model has been the standard turbulent model for the engineering purposes due to its stability and fairly good performance in simulation of many industrial flows. Complete set of continuity and RANS equations with standard *k*-ε closure model (From Fluent 6.3) has been described as follows:

$$\frac{\partial U_i}{\partial t} + U_j \frac{\partial U_i}{\partial x_j} = -\frac{1}{\rho}\frac{\partial P}{\partial x_j} - \frac{2}{3}\frac{\partial k}{\partial x_i} + (\nu + \nu_i)\frac{\partial}{\partial x_j}\left(\frac{\partial U_i}{x_j} + \frac{\partial U_j}{x_i}\right) \quad (3.9)$$

$$\frac{\partial k}{\partial t} + U_j \frac{\partial k}{\partial x_j} = \frac{\partial}{\partial x_j}\left(\nu + \frac{\nu_t}{\sigma_k}\frac{\partial k}{\partial x_j}\right) + (\nu_t)\left[\left(\frac{\partial U_i}{x_j} + \frac{\partial U_j}{x_i}\right)\frac{\partial U_i}{x_j}\right] - \varepsilon \quad (3.10)$$

$$\frac{\partial \varepsilon}{\partial t} + U_j \frac{\partial \varepsilon}{\partial x_j} = \frac{\partial}{\partial x_j}\left(\nu + \frac{\nu_t}{\sigma_k}\frac{\partial k}{\partial x_j}\right) + \left(C_{\varepsilon 1}\nu_t \frac{\varepsilon}{k}\right)\left[\left(\frac{\partial U_i}{x_j} + \frac{\partial U_j}{x_i}\right)\frac{\partial U_i}{x_j}\right] - C_{\varepsilon 2}\frac{\varepsilon^2}{k} \quad (3.11)$$

$$\nu_t = C_\mu \frac{k^2}{\varepsilon} \quad (3.12)$$

$$C_\mu = 0.09, \sigma_k = 1, \sigma_{z1} = 1.3, C_{z1} = 1.44, C_{z2} = 1.92 \quad (3.13)$$

3.2.1.2 Shear stress transport model:

The main shortcoming of two-equation model originates from the linearity of the Boussinesq hypothesis which results in a poor description of rotational mean flows and effects of streamline curvature. Alternatively, Reynolds stress tensor can be calculated by using shear stress transport equations. However, it requires a lot of computing effort as there is six additional equations to calculate six independent Reynolds stresses.

In Fluent, the scalar dissipation rate, ϵ, and turbulent kinetic energy, *k*, are calculated by using the same transport equations used to calculate *k* and ϵ in standard *k*-ε model respectively. The turbulent viscosity, ν_t, is also expressed in the same way as in the standard *k*-ε model (Fluent 6.3).

3.3. Conclusion for model selection

In the modern time, the advance in computer technology has made LES more affordable than before. LES resolves the time dependent motion of large eddies and models only the more isotropic small eddies, therefore, it can inform about transient behavior of a process, such as trailing vortices and macro instability, which cannot be provided by RANS simulation, in the expense of computational cost.

LES is not only more computationally demanding than RANS turbulence model, but it is also more complicated. Available experimental and simulation results are required to determine the grid size in the critical regions. Unfortunately, for rotor-stator mixer, both experimental and simulation results are very limited and not well established.

On the other hand, standard k- ε turbulence model which assumes isotropic turbulence can provide reasonably good predictions of mean velocity components in the stirred tanks although it underestimates turbulent kinetic energy and the rate of energy dissipation. Based on this data, in present work standard k- ε turbulence model is used. Moreover LES is usually started from convergent solution of RANS simulation to speed up its convergence.

3.4 Boundary Conditions and Assumptions

The boundary conditions that have been used are given below:

- No-slip conditions exist such that the fluid velocity would be zero at the walls.
- Fully turbulent flow is assumed in stirred tanks.
- The flow field is not dependent of the fluid viscosity (the viscous heating due to viscous effect is negligible).
- The vortex phenomenon is not present as the surface of the liquid is always considered as flat plane

3.5 Rotation Models:

A 3D modeling simulation required to model the geometry of rotor exactly. There are different approaches available to study the motion of rotor. These approaches must satisfy the computational grid adaptation and available solver method. There are three most commonly used geometry models are following:

1. The rotating Frame model.
2. The multiple reference models.
3. The sliding mesh model.

The first model is used to solve the governing equations for the rotating frame over the entire range of the grid domain. Generally primary rotational component and frame has the same angular velocity for the rotating frame. This model is only applicable for the smooth revolving

surfaces. The angular independent models and axis-symmetrical shapes can be modeled using this model. Vessels with baffles, or inflow-outflow ports could not.

If there is more than one rotating frame the multiple reference models (MRS) will be used for the solution of simulation problem. This approach can be used at the steady state and for complex geometries having more rotating and stationary parts. The interaction between the rotating and stationary parts must be weak for the use of this model. The coordination of rotor-stator assembly may not matter as to obtain the solution of spatial average of power draw (microscopic property). The rotor location should be change to obtain the reasonable solution at the higher interaction.

The sliding mesh model is a time-dependent solution approach and the grid moves physically as according to the rotating component(s) surrounding moves during the solution. There is a zero velocity at which the moving mesh relates to the impeller and shaft, and also for stationary mesh region the velocity of tank, baffles, and other internals is zero. The impeller motion is modeled because the grid surrounding it moves as well, and for impeller-baffle interaction a time-accurate simulation will obtained. There is discontinuity in the grid motion. Rather, it is in small, discrete steps. The convergence reached after an iterative process for the solution of conservation equations.

CHAPTER 4

MODEL DEVELOPMENT AND VALIDATION

The computational fluid dynamics (CFD) model used for the development of new mixer is validated on an existing rotor- stator mixer configuration with square holes. It is observed that that *k-ε* turbulence model is used for rotor stator mixer hydrodynamic prediction. For the validation of the model the simulated results of Utomo et al. (2009) are considered. The geometrical parameters are discussed in section 4.1, grid topology is given in section 4.2, modeling approach in 4.3 and results from the present work are in section 4.4 and 4.5 respectively.

4.1 Geometrical description

For the methodology development and validation the simulation were carried out in L4RT mixer proposed by Utomo et al. (2009). The L4RT model mixer is a 4 rotor blade with 28.2 mm diameter. There are 92 holes of 2.6×2.4 (width to depth ratio) in the stator section. Upper area of the rotor swept volume is closed with 25.4 mm diameter circular open section in the bottom. The gap between the rotor blade and stator wall is settled at 0.175 mm. Diameter of the implied tank is 150 mm with 150 mm height as shown in Fig. 4.1(c). The geometry was created in commercial computational fluid dynamic software Fluent 6.3.

4.2 Grid topology

The HSM geometry comprises of stator, rotor and mixing vessel. Due to the complexity in the geometry the rotor-stator mixer, it is divided in the following zones:

- rotor fluid region,
- fluid in the gap between the rotor and stator, and
- stator fluid region,

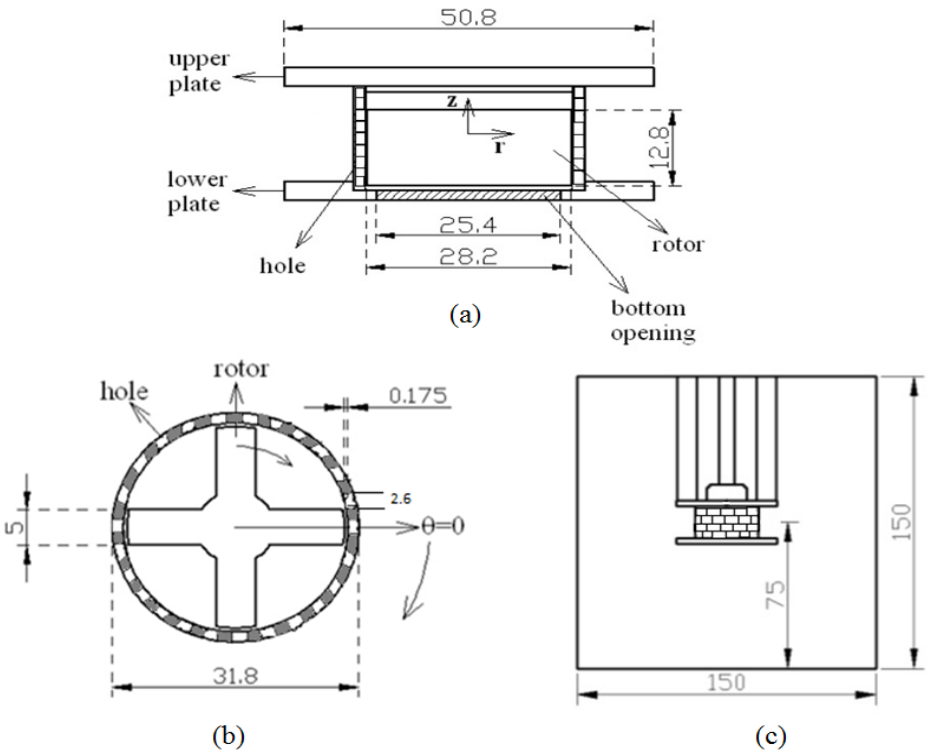

Fig. 4.1: (a) Lateral view of L4RT Silverson mixer, (b) Top view of L4RT Silverson mixer, and (c) Tank with L4RT Silverson mixer.

For validation purpose geometry construction and boundary condition description are important factors. Besides this the proper grid formation also plays an important role. On the basis of final grid testing meshing has been done in the prescribed format as described in Pacek et al. (2009). In the present work similar grid nodes and number of cells are applied as was used by Pacek et al. (2009). The number of computational cells varied from 1.1 to 1.4 million. The grid topologies of different zones are shown in Figs. 4.2-4.4 and grid details are given in Table 4.1.

Table 4.1 Grid details in various zones.

Zone	Meshing scheme	Total mesh volume
Rotor fluid zone (Fig. 12)	Hybrid (Tetrahedral/Hexahedral)	80040 x4
Fluid in the Gap between the rotor and stator (Fig. 13)	Hybrid (Tetrahedral/Hexahedral)	112320
Stator fluid region (Fig. 14)	Hexahedral	320x92 = 29440

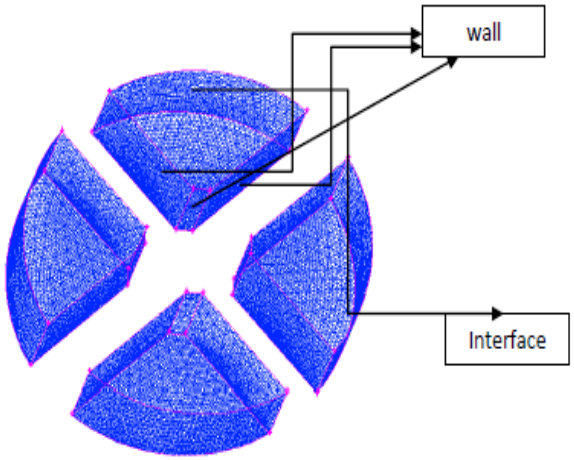

Fig. 4.2 Rotor fluid grid topology

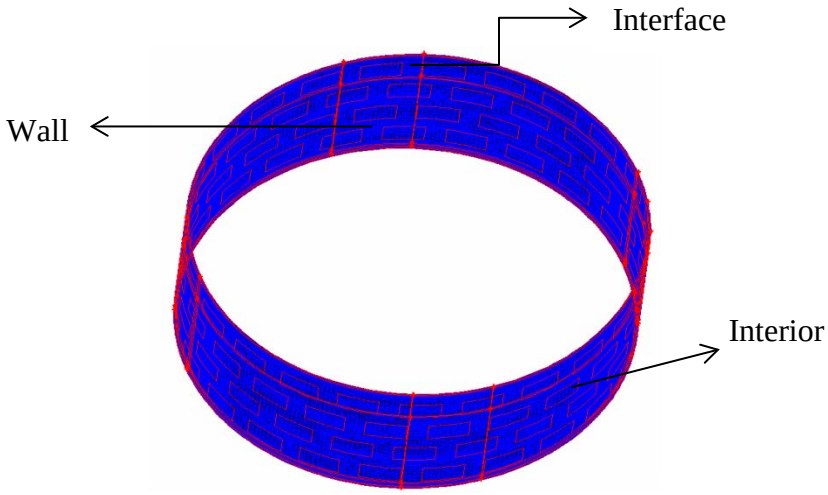

Fig. 4.3 Gap fluid grid topology

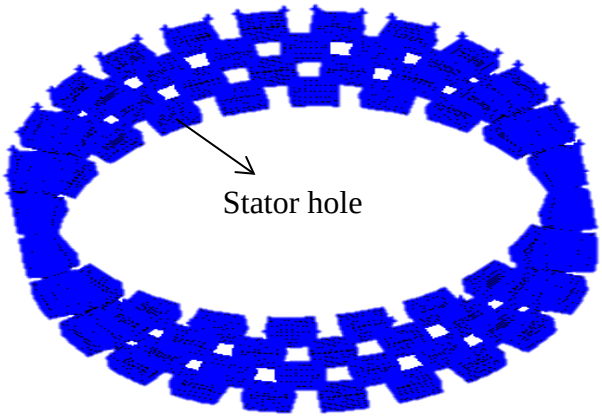

Fig. 4.4 Stator fluid grid topology

The HSM domain consisted of 600,000 non-uniformly distributed hybrid cells (tetrahedral and hexahedral) within the bulk tank region and 400,000 hybrid cells within the rotor- stator region. The gap between rotor and stator was divided into 5 hexahedral cells and the interface between rotating and stationary frames is located at the middle of the gap.

4.3 Modeling approach

The simulation was carried out using Fluent 6.3, started with steady state multiple references frames and then continued with transient sliding mesh. Standard k-ε turbulence model was used to model the turbulence with enhanced wall function, which can describe the flow in viscous sub layer, buffer region and fully turbulent outer region. The pressure and convection terms were coupled using SIMPLE algorithm. The simulation was started directly with the sliding mesh method with 120 time steps per rotor revolutions and the simulations were run for 100 rotations. In each time step, the solution is converged with residuals below10^{-3}, which took about 10 minute of CPU time.

4.4 Results and discussion

For the model validation present results are validated with the experimental and CFD results of Utomo et al. (2009). On the basis of these results extensive study of the mixer has been performed in terms of flow fields. The rotor is settled on the constant speed of 4000 rpm for resultant simulation.

4.4.1 Torque fluctuation

The variation of torque with respect to blade position shows a amplitude fluctuation and the present work results shows a good agreement with the results of Utomo et al, (2009). The fluctuation of the torque from the average torque with respect to blade position is shown in Fig. 4.5. It can be seen that the fluctuation is very less in the torque.

There are 4 rows containing 23 holes in a row and alternate row is superimposed on each other so that the fluctuation created by row is counterbalance by the above row and hence the fluctuation in the torque is less.

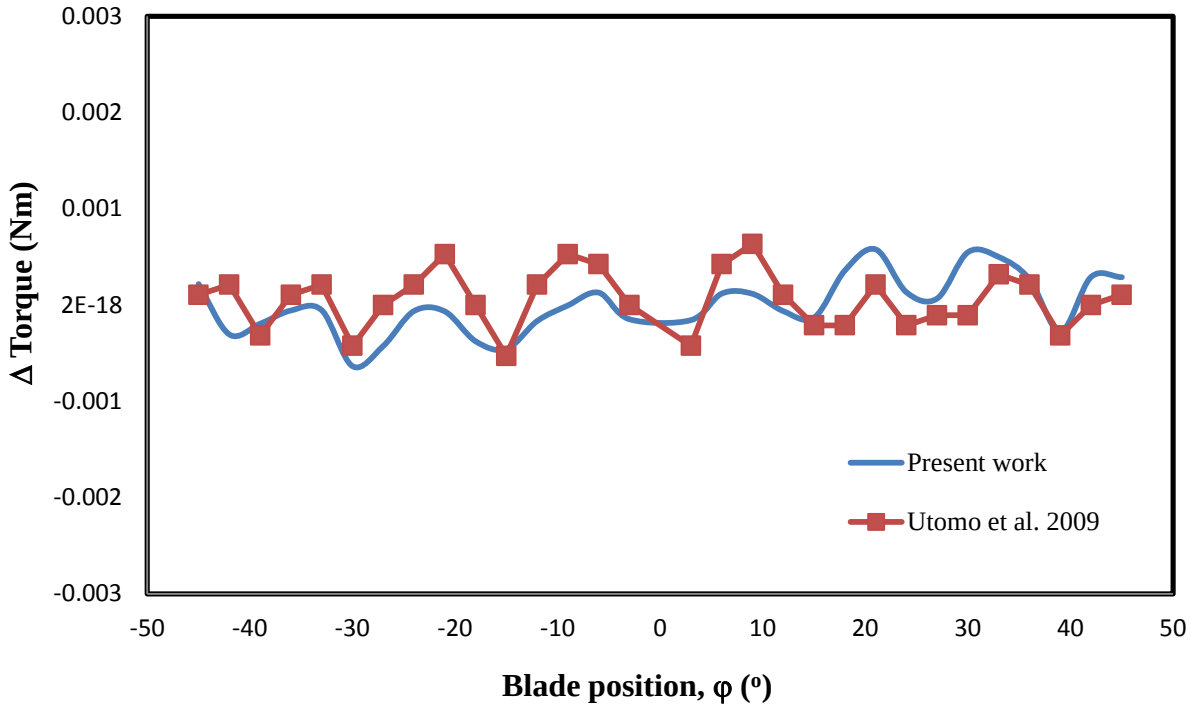

Fig. 4.5 Variation of fluctuating torque with the blade position

4.4.2 Mass flow rate

From Fig. 4.6 it can be seen that the fluctuation in the flow rate is constant with the blade position. There is a deviation of 1.5% in the present work from the numerical prediction of Utomo et al, (2009).

From the Figs 4.5 and 4.6 it can be seen that the fluctuation of torque and mass flow rate is constant for the square holes stator. The amplitude of fluctuation is zero for the square holes stator. The reason for the less fluctuation in flow rate is same as for the torque fluctuation.

The power number and mass flow rate in the square holes HSM were predicted at 4000 rpm and compared with the CFD results of Utomo et al, (2009) (Table 4.2). The Flow number (*Fl*) and Power number (P_o) were calculated using Equations 4.1 and 4.2, respectively.

$$Fl = Q/ND^3 \qquad (4.1)$$

where Q is volume flow rate, N represents rotor speed and D is the rotor diameter and

$$P_o = P/\rho N^3 D^5 \qquad (4.2)$$

where P is power drawn, and ρ is density of fluid.

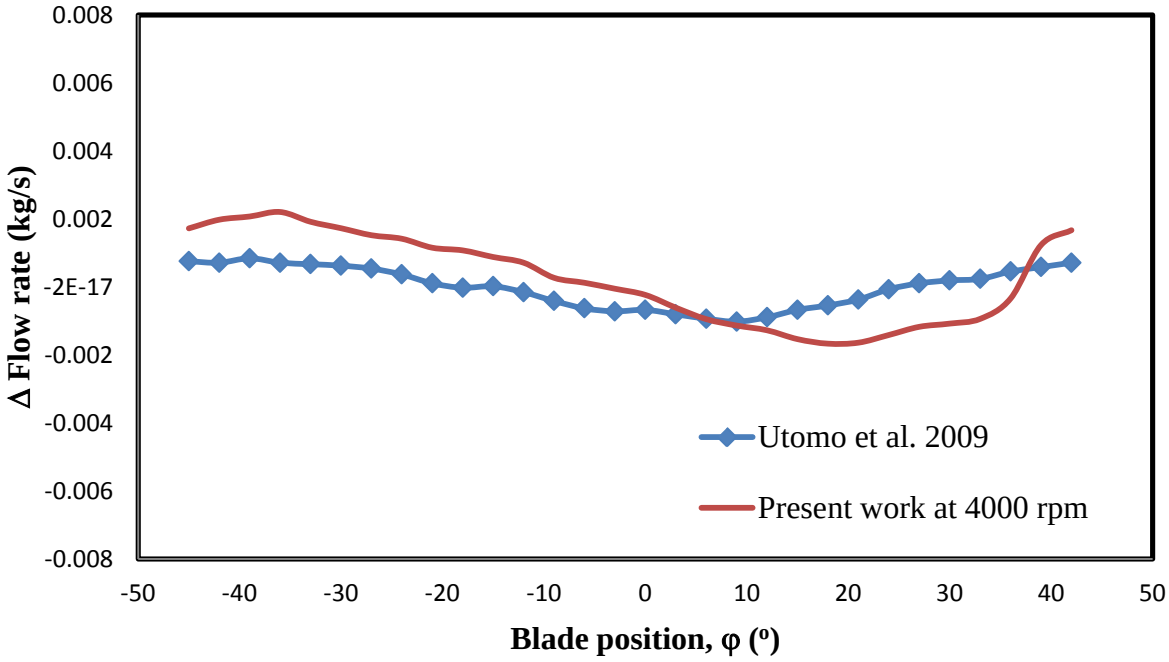

Fig. 4.6 Variation of fluctuating flow rate with blade position

Table 4.2 Comparison of different parameter for square holes stator head at 4000 rpm.

Stator	Power Number (Simulated)	Power Number (Utomo A. et al, 2009)	% difference	Flow Rate (kg/s) (Simulated)	Flow Rate (kg/s) (Utomo A. et al, 2009)	% difference
Square head at 4000 rpm	1.7	2.05	17.1	0.383	0.389	1.5
			Pumping Efficiency, E_p (10^{-6}) = 12.68			
			Flow Number (Fl) = 0.256			

Table 4.2 shows that the above results obtained in the present work are in good agreement with the CFD results of Utomo et al, (2009). From Table 4.2, it can be seen that there is deviation of 17.1% and 1.5% on Power number and flow rate, respectively.

4.4.3 Pumping efficiency

Pumping efficiency of the rotor stator mixer is observed low as compared to the Rushton turbine due to its poor mixing in bulk region (Bakker et al., 1990). Pumping efficiency (E_p) is calculated using Equation 3.3.

$$E_p = \frac{Q^3\rho}{PT^4} = \frac{Fl^3}{P_0}\left(\frac{D}{T}\right)^4 \tag{3.3}$$

where T represents the diameter of the tank and Fl is the Flow number, P_o is the Power number which has constant value for Re $>10^4$.

The pumping efficiency reported in the present work is very low as compared to Ruston turbine and the power drawn is very high. Therefore lower power number high energy dissipation is required to develop a new mixer. The pumping efficiency calculated in Table 4.2 is 12.68×10^{-6} which is very low compared to the Ruston turbine.

4.4.4 Energy dissipation rate

The rate of energy dissipation for the square holes stator was calculated at the rotor speed of 4000 rpm and compare with the existing results of Utomo et al, (2009). The simulated results were in good agreement with the available results and are shown in Fig. 4.7.

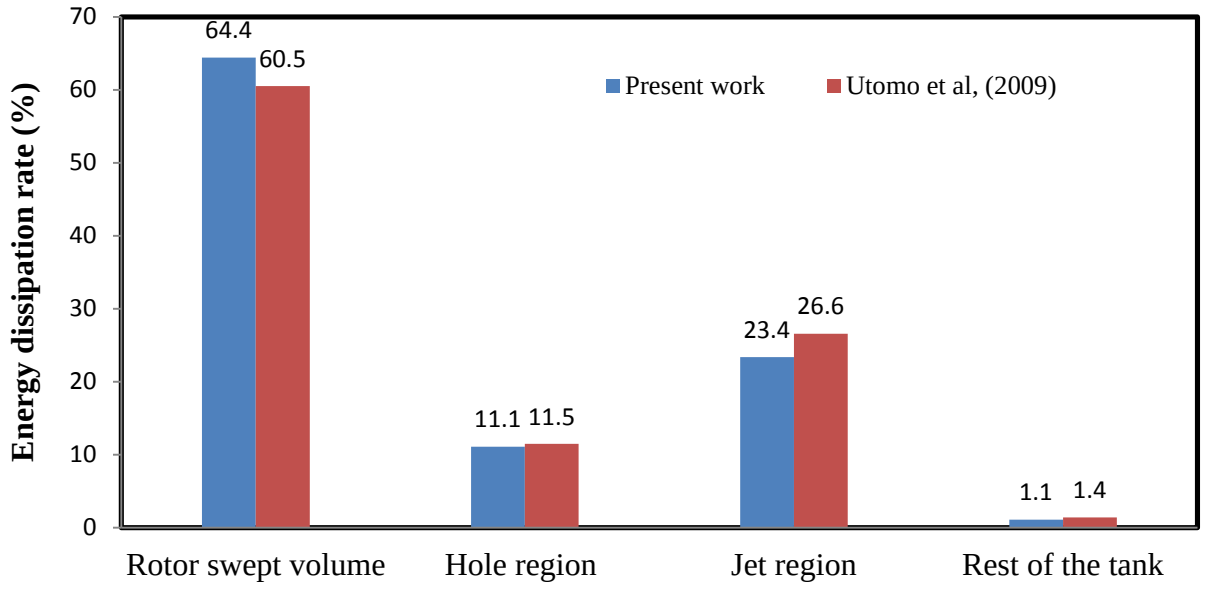

Fig. 4.7 Comparison of energy dissipation rate for square holes stator assembly at 4000 rpm.

Fig. 4.7 shows that the rate of energy dissipation in the rotor swept region is very high as compared to the other region. Different region defined in the model are the holes region is defined as the area covered by all the stator holes, jet region is the area same as the height of stator head over a distance of r = 15.9 mm and the rest is tank area.

The present predictions for energy dissipation are compared with Utomo et al, (2009) and it can be concluded that there is less difference in the present work prediction and the available results: -3.9 for the rotor volume, 0.4 for the holes region, 3.2 for the jet region and 0.3 for the rest of tank.

4.5 Comparison of results at 2000 rpm and 4000 rpm

As there are no results available for the square holes stator at the different rotor speed, therefore the fluctuation of torque, mass flow rate and rate of energy dissipation are further carried out at the rotor speed of 2000 rpm. The comparison of the torque fluctuation and mass flow rate fluctuation at 2000 rpm and 4000 rpm are shown in the Figs. 4.8-4.9. The energy dissipation rate in different regions is given in Table 4.4.

From Fig. 4.8 it can be seen that the fluctuation of torque with the blade position at the rotor speed of 2000 and 4000 rpm and the amplitude fluctuation is near to zero. It is clear that at 4000 rpm the fluctuation is high as compared to 2000 rpm.

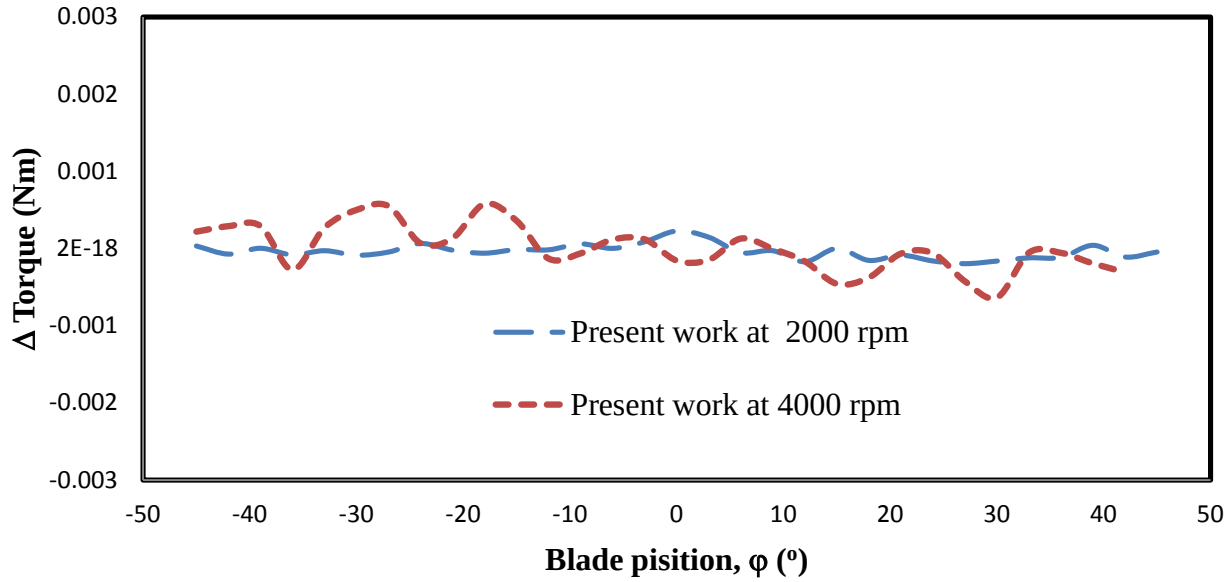

Fig. 4.8 Comparison of torque fluctuation at the different rotor speed relatives to the blade position.

The variation of mass flow rate with the blade position was calculated at the speed of 2000 and 4000 rpm is shown in Fig. 4.9. It was observed that the fluctuation there were less as for 2000 rpm as compared to the torque fluctuation calculated at the speed of 4000 rpm.

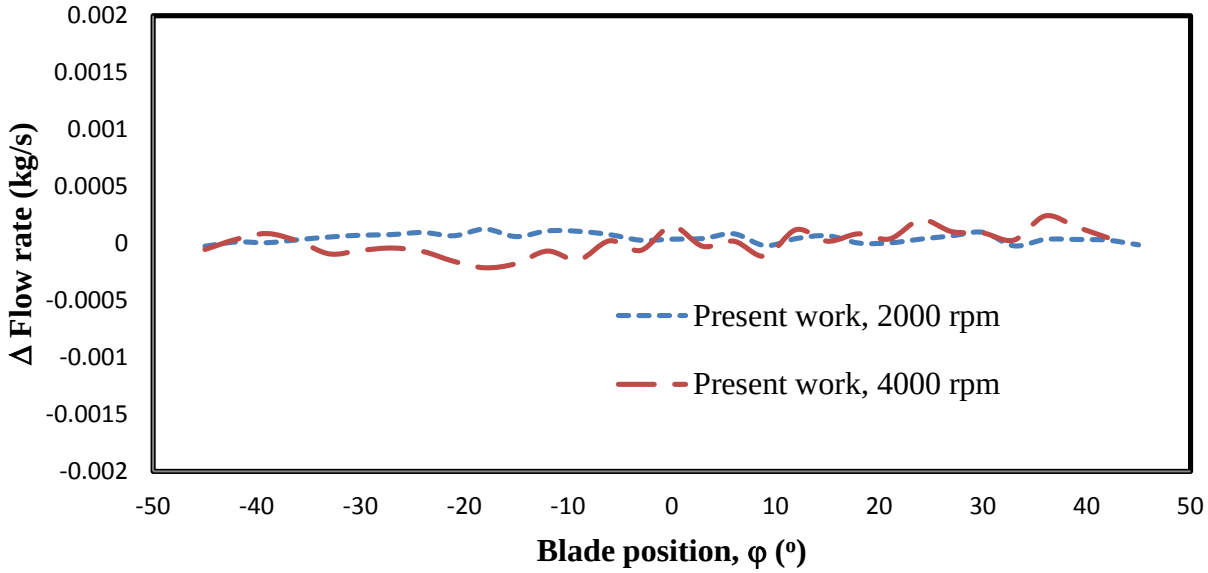

Fig. 4.9 Comparison of flow rate fluctuation at the different rotor speed relatives to the blade position.

The power number and mass flow rate were compared with the results of square holes stator at the rotor speed of 4000 rpm and the Flow number (*Fl*) and Power number (P_o) were calculated using the equations 4.1 and 4.2 respectively and is shown in Table 4.3.

The rate of energy dissipation is also compared at the different rotor speed and it has been observed that the rotor swept volume energy dissipation rate is high but less in the jet region at the 4000 rpm as shown in Table 4.4.

Table 4.3 Comparison of different parameters at the different rotor speed of 2000 and 4000 rpm.

Rotor speed (rpm)	**Power Number (P_o)**	**Flow Rate (kg/s)**	**Flow number (*Fl*)**	**Efficiency E_p (10^{-6})**
2000	1.69	0.194	0.260	13.01
4000	1.7	0.383	0.258	12.68

Table 4.4 Comparison of energy dissipation rate at the different rotor speed of 2000 and 4000 rpm.

Rotor speed (RPM)	Rotor swept volume	Hole region	Jet region	Rest of the tank
2000	60.4	13.4	24.5	1.7
4000	64.4	11.1	23.4	1.1

From Table 4.4 it has been concluded that as the rotor speed increases the rate of energy dissipation also increases and in rest of the regions the energy dissipation rate is less. The volume swept by the rotor increases with the rotor speed.

CHAPTER 5

NUMERICAL MODELING OF NOVEL MIXER

The L4RT mixer penetrates straight in the mixing vessel. In the present work the existing L4RT mixer is modified to have further penetration in the mixing vessel. The upper and lower two rows of the jets are tilted to get the deep penetration inside the mixing vessel. In this chapter the details of the proposed geometry are discussed in section 5.1. In section 5.2 the grid topology of the proposed design is reported. The modeling approach and results are reported in section 5.3.

5.1 Geometry description

Bulk geometry is same as described in the earlier structure diameter of stator holes is 1.8 mm and stator having a diameter of 31.8 mm. Rotor dimension considered were similar as discussed in the Utomo et al. (2009). The structure of the stator geometry was modified for further jet penetration in the mixing vessels. In the proposed geometry 35 holes in each row with 6 rows were introduced in the stator and there is a 22.5^0 angle inclinations of stator holes for upper and lower rows in the positive and negative z-direction, respectively. Sequence of the holes follows alternative way in vertical direction. To reduce the stator wall forces for the restrictions of the jets the stator plate size was reduced to 30 mm. The proposed mixer configurations are shown in Fig.5.1 to Fig.5.3.

5.2 Grid topology of the proposed geometry

On the basis of the complexity, the geometry was divided in the following zones:

- rotor fluid region,
- fluid in the gap between the rotor and stator,
- stator fluid region,
- inner bulk fluid region, and
- outer bulk fluid region.

For results comparison the similar geometry construction, boundary conditions and grid topology is considered as in the case of L4RT mixer.

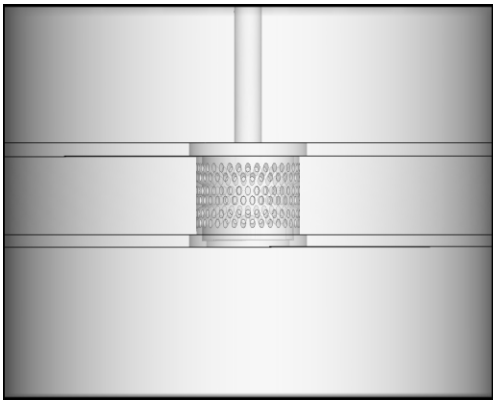

Fig. 5.1 Tank with proposed mixer

Fig. 5.2 3D view of rotor-stator assembly

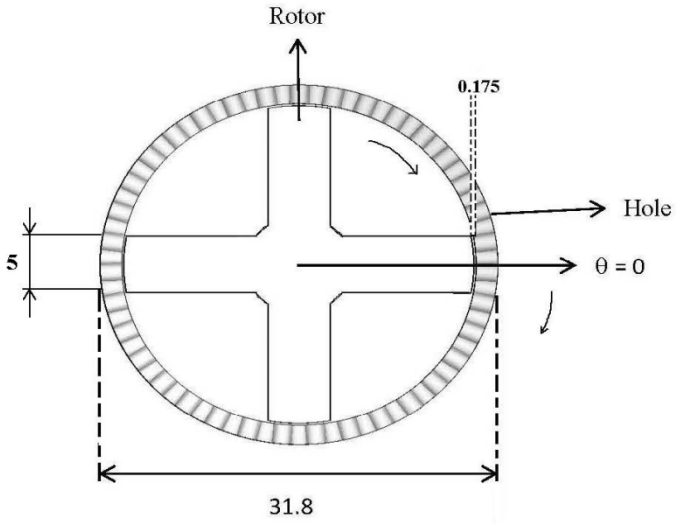

Fig. 5.3 Top view of the proposed rotor-stator mixer assembly

Table 5.1 Grid details in various zones.

Zone	Meshing scheme	Total mesh volume
Rotor fluid zone (Fig. 5.4)	Hybrid (Tetrahedral/Hexahedral)	25700 x 4
Fluid in the Gap between the rotor and stator (Fig. 5.5)	Hybrid (Tetrahedral/Hexahedral)	15544
Stator fluid region (Fig. 5.6)	Hybrid (tetrahedral/hexahedral)	78596

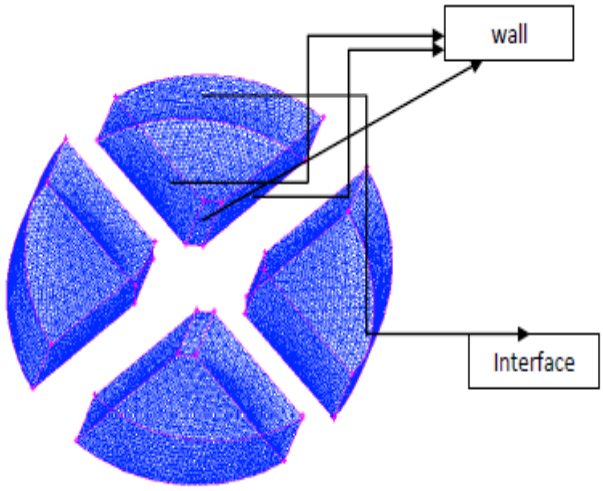

Fig. 5.4 Grid topology of rotor fluid zone in the proposed geometry

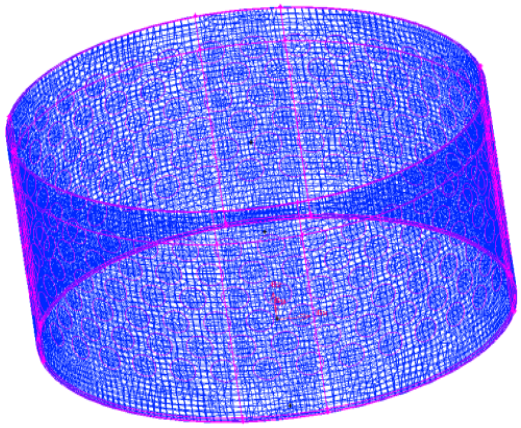

Fig. 5.5 Grid topology of gap zone in the proposed geometry

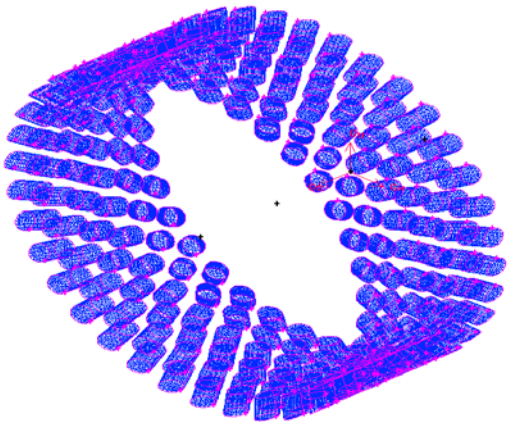

Fig. 5.6 Grid topology of stator fluid zone in the proposed geometry

Table 5.2 Grid details in the Bulk region

	Inner bulk fluid	Outer bulk fluid	Below bulk fluid
Mesh type	Hybrid cells	Hybrid cells	Hybrid cells
Total mesh node	39486	78623	46614
Total mesh volume	199970	380249	199240

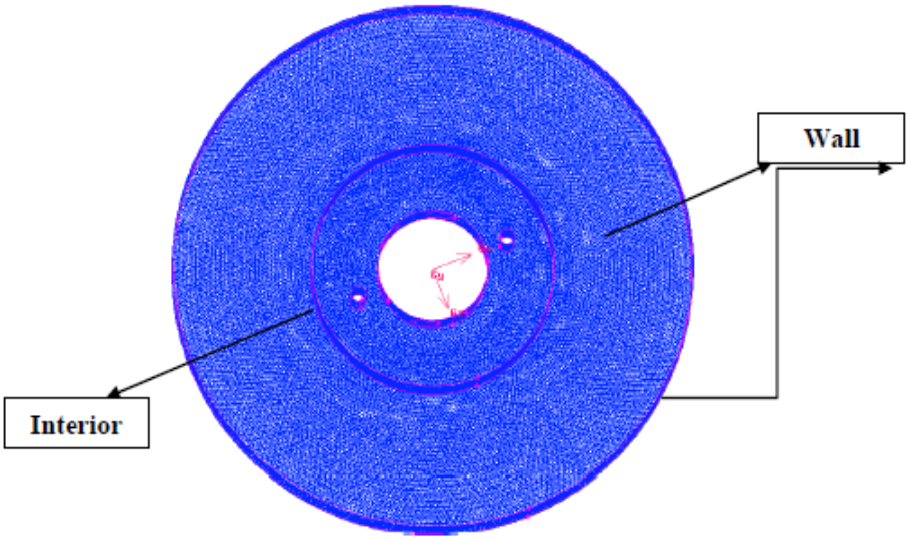

Fig. 5.7 Grid topology of bulk region in the proposed geometry

5.3 Modeling approach

The computational model was fully 3D geometry consisted of about 700,000 non-uniformly distributed hybrid cells (tetrahedral and hexahedral) in the bulk tank region and about 600,000 hybrid cells inside the rotor-stator region. The gap between rotor and stator was divided into 5 hexahedral cells and the interface between rotating and stationary frames was located at the middle of the gap.

The simulation was carried out using control volume finite difference method (CVFDM) using a commercial software Fluent 6.3. Initially computations were carried out with steady state multiple references frames and then continued with transient sliding mesh. Standard k-ε turbulence was used to model the turbulence and enhanced wall function, which can describe the flow in viscous sub layer, buffer region and fully turbulent outer region. The pressure and convection terms were coupled using SIMPLE algorithm. The time step in the transient sliding

mesh simulation was 1/120 of the rotor revolution time. In each time step, the solution is converged with residuals below 10^{-3}, which took about 10 minute of CPU time.

The proposed geometry was simulated at the different rotor speed of 2000 rpm, 4000 rpm and 6000 rpm and the variation of torque, mass flow rate with respect to blade position was simulated. The computed results were compared with the prediction of Utomo et al, (2009) and with the simulated results of square stator head assembly. The fluctuation in torque and mass flow rate with respect to blade position are shown in Figs.5.8 and 5.9.

5.3.1 Torque fluctuation

Fig. 5.8 shows the deviation of the torque from the average torque with respect to blade position in the novel mixer at 4000 rpm. In Fig. 5.8 the computed results in novel mixer is compared with the prediction of Utomo et al, (2009) and present work in square holes head high shear mixer. It can be seen from Fig. 5.8 that the fluctuations in proposed novel geometry is more as compared to square holes geometry.

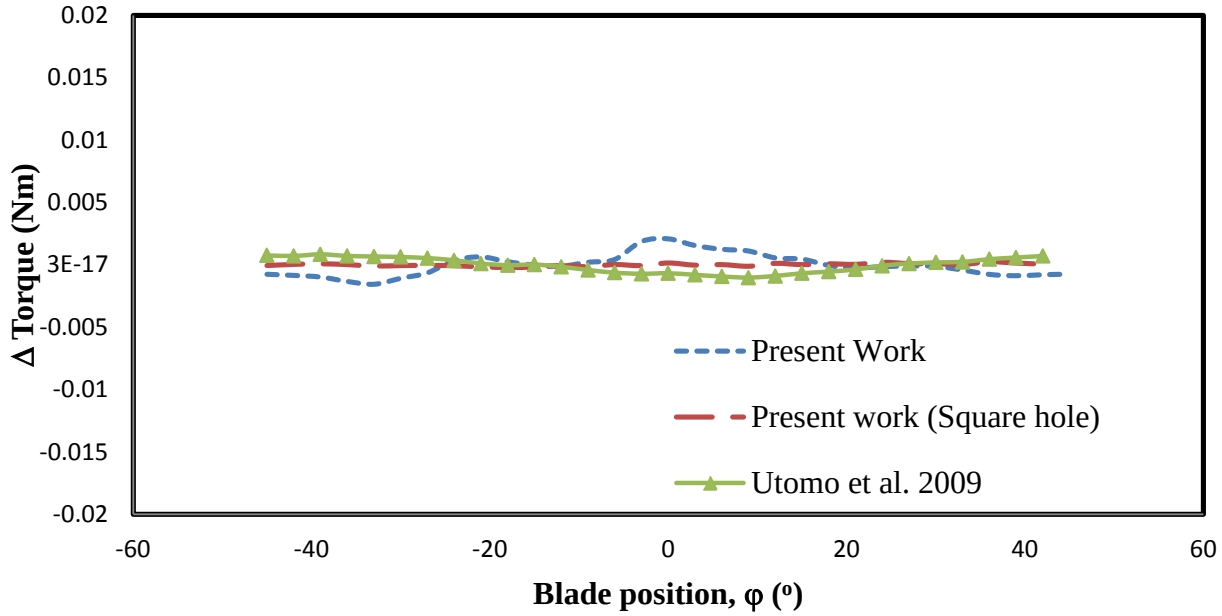

Fig. 5.8 Variation of torque fluctuation with blade position

5.3.2 Mass flow rate

The fluctuation in mass flow rate with respect to blade position from the time averaged value is shown in Fig. 5.9. It can be seen from Fig. 5.9 that the mass flow rate fluctuation in the proposed

novel mixer is higher as compared to the square holes head geometry. However the mass flow rate obtained in proposed novel mixer is high, which may results in better mixing in the rotor region. The different parameter of proposed novel mixer geometry with disintegrated head at 4000 rpm is reported in Table 5.3.

Table 5.3 Comparison of different parameter for the proposed geometry at 4000rpm.

Stator	Power Number (Present study)	Flow Rate (kg/s) (Present study)	Flow number (Present study)	Pumping efficiency, *Ep* (10^{-6})
Disintegrated head at 4000 rpm	1.66	0.342	0.229	9.04

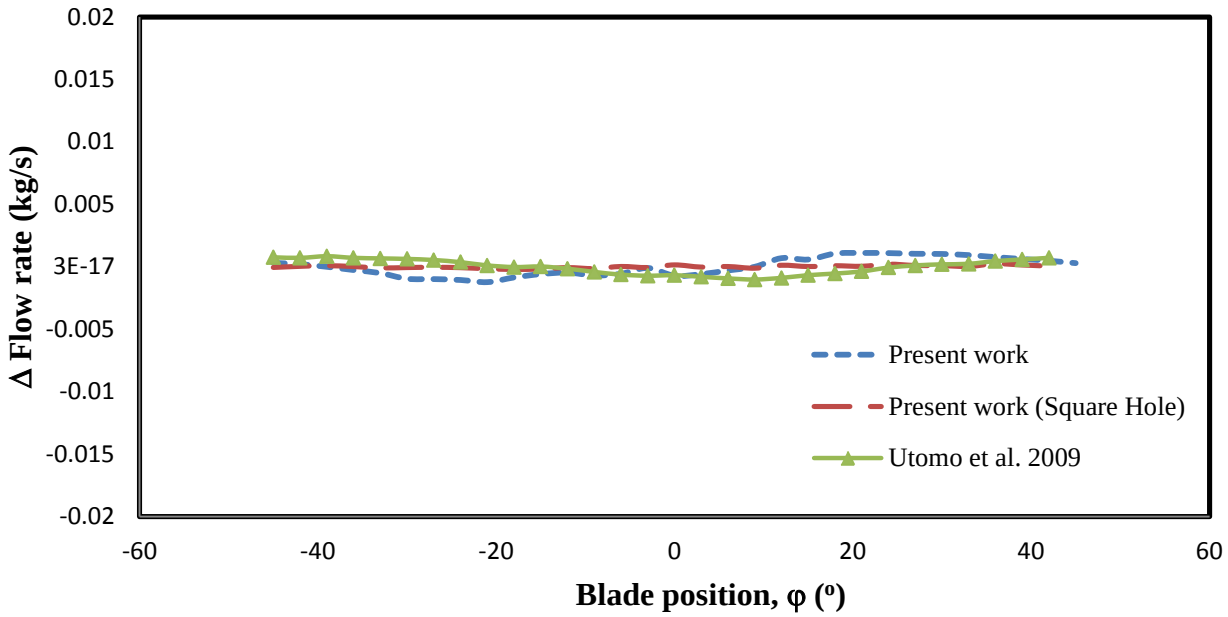

Fig. 5.9 Variation of flow rate with of blade position

From Table 5.3 it can be seen that the pumping efficiency in the proposed novel mixer is sufficient as compared to the pumping efficiency of the square holes head assembly at the same rotor speed of 4000 rpm. The flow number and power number has been calculated using equation 4.1 and 4.2 respectively.

5.3.3 Pumping efficiency

Pumping efficiency is calculated from the equation 4.3. It was observed that the pumping efficiency of the rotor stator mixer is low as compared to the Rushton turbine due to its poor mixing in bulk region (Bakker et al., 1990). The pumping efficiency of proposed novel mixer is in a good agreement with the square holes head mixer at the same rotor speed.

5.3.4 Energy dissipation rate

In the present work the comparison of the energy dissipation rate with respect to the rotor speed has been studied and the simulated results at 4000 rpm in the novel proposed mixer were compared with the results of Utomo et al, (2009) and the present work for the square holes rotor-stator assembly (Fig. 5.10).

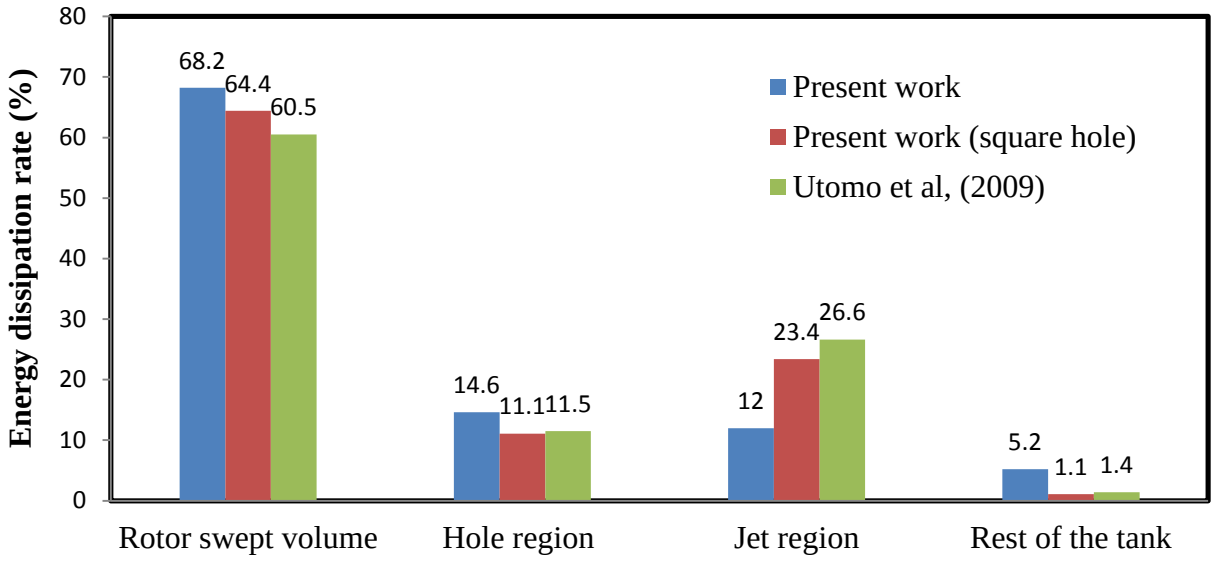

Fig. 5.10 Comparison of energy dissipation rate for rotor-stator assembly at 4000 rpm

From Fig. 5.10 it can be concluded that the rate of energy dissipation is high in the rotor region, the holes region and is less in the jet region the rest of the tank for the proposed novel mixer at rotor speed of 4000 rpm. As the number of holes in the proposed novel mixer is more as compared to the existing mixer, therefore the rate of energy dissipation is more in the holes region of novel mixer. Jet region dissipation rate is less in the novel mixer because the intensity

of turbulence in the proposed mixer is less in the jet region as compared to the square holes mixer. There are four layers of holes in the square holes and in the proposed mixer there are only two layers of holes in the jet region. The upper two layers of holes in the novel mixer are tilted with an angle of 22.5^0; the two lower layers of holes are at an angle of -22.5^0 and rest two layers are at the 0^0.

5.4 Results and discussion

The fluid flow and mixing analysis in the proposed novel mixer (HSMs) was carried out at different rotor speed, i.e. 2000 rpm, 4000 rpm, and 6000 rpm. In this section the results of proposed HSM mixer are discussed and compared with the existing RSM. The results were analyzed in term of fluctuation of the torque (section 5.4.1), mass flow rate with respect (section 5.4.2), the rate of energy dissipation at the different rotor speeds and (section 5.4.3), the pumping efficiency (section 5.4.4). The comparison of the proposed novel mixer to the existing mixer has been discussed in the section 4.3 at the rotor speed of 4000 rpm. It has been found that the proposed novel mixer is highly efficient. So that to compare these different parameters the proposed novel mixer was simulated at the different rotor speed by keeping the same modeling approach. The comparison of torque fluctuation and mass flow rate at the different rotor speeds are discussed and shown in Fig. 5.11 and Fig. 5.12.

5.4.1 Torque fluctuation

The variation of fluctuating torque with respect to the blade position at different rotor speed is shown in Fig. 5.11. It has been observed that the fluctuation in the torque at the 6000 rpm rotor speed is higher as compared to 2000 rpm and 4000 rpm.

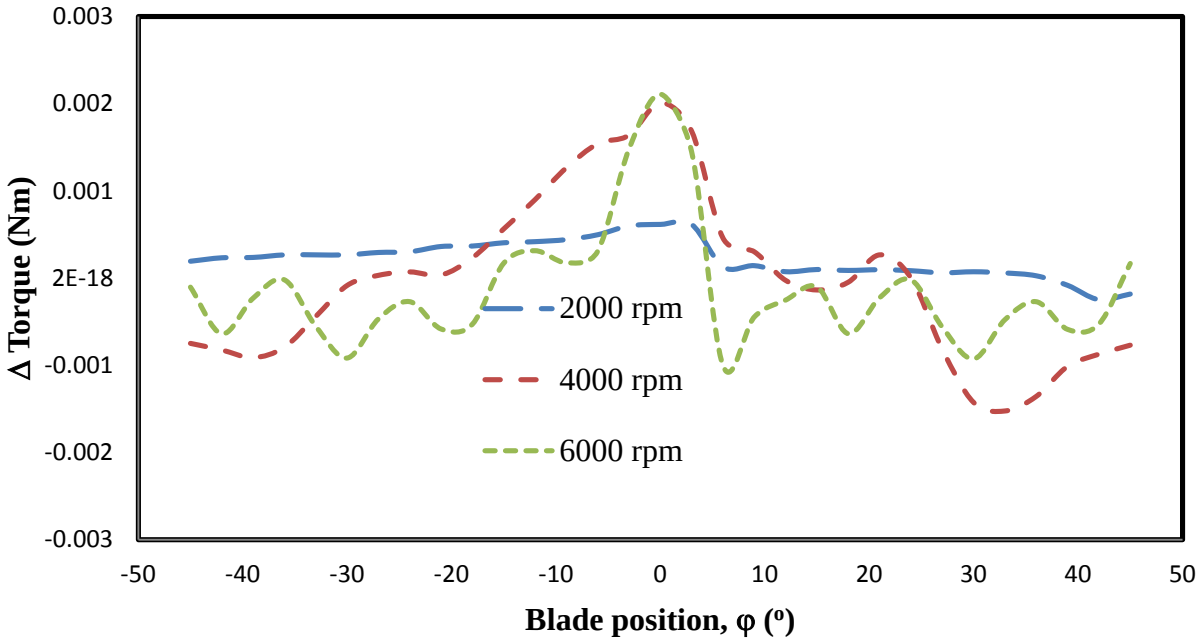

Fig. 5.11 Comparison of fluctuating torque at the different rotor speed with respect to the blade position in the novel proposed mixer.

At the 2000 rpm the amplitude of fluctuating torque is approximately zero and there is some disturbance when the blade position changed from negative to positive direction. At the rotor speed of 6000 rpm the fluctuation amplitude has maximum value and the same maxima can be seen for the speed of 4000 rpm.

5.4.2 Flow rate fluctuation

At 6000 rpm the mass flow rate vary the most as compared to the 4000 rpm and 2000 rpm. From Fig. 5.12 it can be seen that the value changes at the minimum negative value to the maximum positive value at the 6000 rpm. As the rotor speed increased the amplitude in the fluctuation increased and the deviation from positive to negative is also increased.

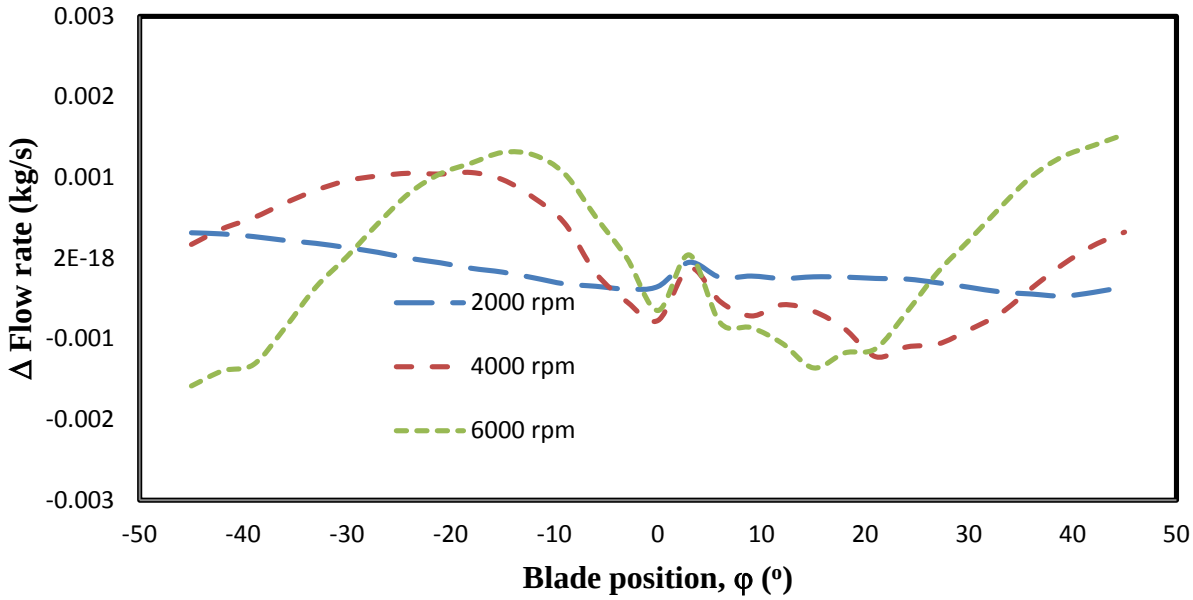

Fig. 5.12 Comparison of flow rate fluctuation at the different rotor speed with respect to the blade position in the novel proposed mixer

5.4.3 Energy dissipation rate

The rate of energy dissipation is compared at different rotor speed in for different region in the proposed novel mixture and is reported in Table 5.4

Table 5.4 Comparison of energy dissipation rate for the proposed geometry at different rotor speed.

Rotor speed (rpm)	Rotor swept volume	Holes region	Jet region	Rest of the tank
2000	65.1	17.1	12.9	4.9
4000	68.2	14.6	12.0	5.2
6000	70.1	13.7	10.2	6.0

From Table 5.4 it can be concluded that the maximum energy dissipation occurs in the rotor swept region at the different rotor speeds. The rate of energy dissipation increased with increase

in the rotor speed in the rotor swept volume region and the bulk (rest of the tank) region. In jet and holes (stator) region energy dissipation rate decreased as the rotor speed increased.

The mass flow rate, power number, flow number and pumping efficiency were calculated for the proposed novel mixer at the different rotor speed and are given in the Table 5.5. It can be concluded from the Table 5.5 that the power number and pumping efficiency decreases as rotor speed increase but mass flow rate increases.

Table 5.5 Comparison of different parameters for the proposed geometry at different rotor speed (2000rpm, 4000 rpm and 6000 rpm).

Rotor speed rpm	**Mass flow rate (kg/s)**	**Power number (*Po*)**	**Flow Number (*Fl*)**	**Efficiency (*Ep*) $*10^{-6}$**
2000	0.173	0.98	0.231	15.8
4000	0.346	1.37	0.231	11.3
6000	0.499	1.68	0.223	8.3

CHAPTER 6

MIXING CHARACTERZATION IN SQUARE HOLES AND PROPOSED NOVEL RSM

Mixing process is very significant in all major process industries, energy, minerals mining, chemical industries, pharmaceuticals production, food and metallurgical processing etc. Computational fluid dynamics (CFD) is a very useful tool to understand the mixing processes in detail. Industrial Mixing using high shear mixer is actually dispersing, or transporting, one phase or ingredient (liquid, solid, gas) into a main continuous phase (liquid), with which it would normally be immiscible. CFD aids in correct analysis of mixer style and application, however it cannot be used as a stand-alone style tool. Mixer analysis not solely includes optimizing the blade dimensions, however conjointly includes mechanical design of impeller and tank, tank internals design (i.e., baffles, coils) etc. Significant improvements of the design capability and reliability of mixing tank may be possible with advancement in computational fluid dynamics (CFD) simulation. The mixing approach is discussed in section 6.1 and results obtained in the proposed novel mixer and existing mixer are discussed are in section 6.2.

6.1 Mixing approach

The mixing characteristics can be compared in a mixer by using two different kinds of residence time distribution (RTD) calculation and they are given as

1. Species transport model.
2. User defined scalar (UDS) transport model.

For the present study the species transport model without any reaction is used to study the mixing characteristics in the proposed novel mixer and the existing square holes rotor-stator mixer. Basically the *residence time* is the time that can be spend by a molecule within the reactor or mixer. In the species transport model a tracer is used as a species and modeled as the same as species. In this method all the properties of tracer are same as the used liquid. The density of the

tracer has been varied according to the volume-weighted-mixing-law and the viscosity remains constant as of water. The defined tracer has a volume of 0.015% of the total volume of the tank. The tracer input at the center of the tank in the rotor below interior.

A total of seven different positions are drawn in the tank to study the uniform distribution of the species. The area-weighted average of the mass fraction of the tracer or species monitored at these different points with respect to the flow time for the proposed novel mixer and existing mixer at the different rotor speeds. The flow time is the mean residence time of all the molecules of the tracer. The converged solution of the first order upwind has been used for the next 100 rotations of the rotor. The governing species equation of the tracer has been solved by using the QUICK scheme. The different positions used to analyze the RTD curve are shown in Fig. 6.1a and Fig. 6.1b for proposed novel mixer and existing mixer.

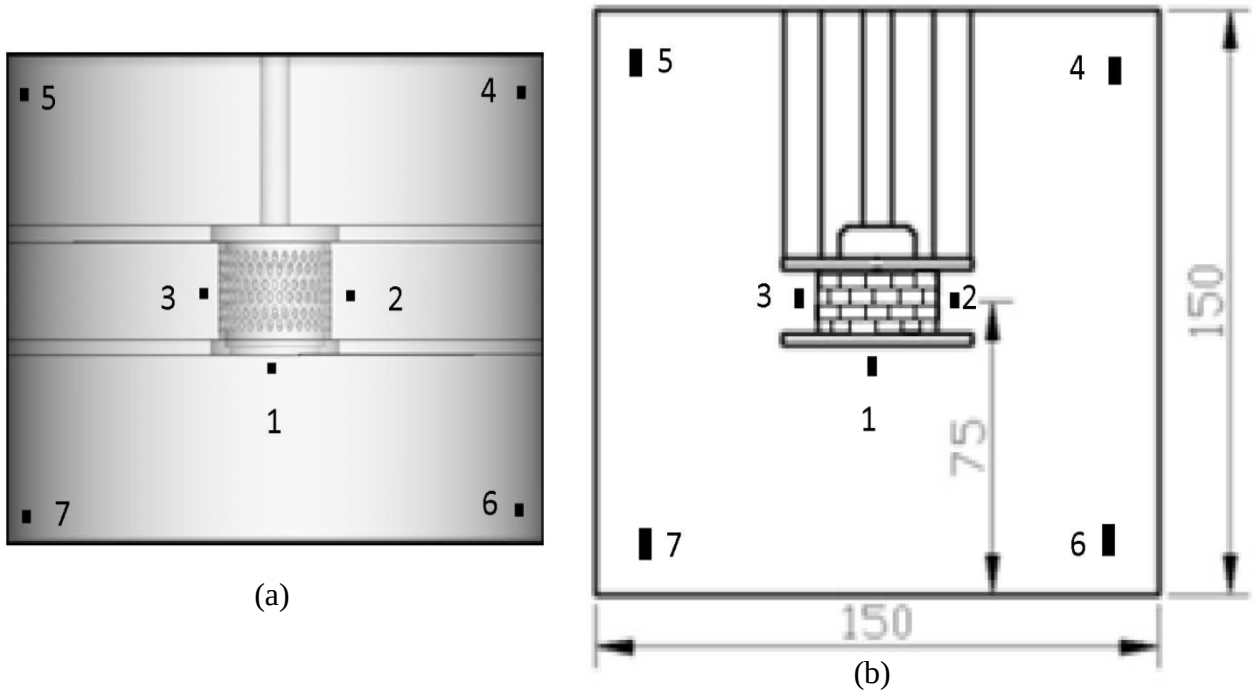

Fig. 6.1 (a) Proposed novel mixer, and (b) Square Rotor stator L4RT Silverson mixer (Source: Utomo et al., (2009)

The tracer is input at point 1 in both the geometry and the monitored at points 1 to 7. The mass fraction of the tracer was monitored and compared at these different points for the different rotor

speeds. The different points considered for the monitoring of tracer concentration in the proposed novel mixer and the existing square rotor stator mixer were same.

The analysis of RTD curves and contours of species distribution in the tank at the vertical plane in both the geometry are discussed in the section 6.3. The dimensions of the different points are given (Table 6.1) in Cartesian coordinate (x y z) system for the proposed novel mixer.

Table 6.1 Dimensions of the different points in Cartesian coordinate (x y z) system.

Region	X	Y	Z
Point 1	0	0	0
Point 2	20.3	0	8.25
Point 3	-20.3	0	8.25
Point 4	70	0	38
Point 5	-70	0	38
Point 6	70	0	-24
Point 7	-70	0	-24

6.2 Results and discussion

6.2.1 Tracer concentration in square holes RSM

The mass fraction of tracer with respect to the flow times for the existing mixer is shown in Figs 6.2-6.5 at different points and rotor speed (2000 rpm and 4000 rpm). The uniformity of the species mass fraction in the existing mixer is also observed in the Fig. 6.6 and Fig. 6.7 on a vertical plane in the middle of the tank at rotor speed of 2000 rpm and 4000 rpm.

From Fig. 6.2 it can be seen that the flow time of the tracer at the rotor speed of 2000 rpm and 4000 rpm are nearly the same. The mass fraction of tracer is increased from zero to maximum and then decreased to the minimum value. From Fig. 6.2 it can be seen that the mass fraction is

zero at 1.86 second for the rotor speed of 4000 rpm and 1.89 second for the 2000 rpm. Therefore it can be concluded that the mixing is uniform and can be achieved faster at higher at 4000 rpm as compared to 2000 rpm. Hence better mixing is attained at 4000 rpm.

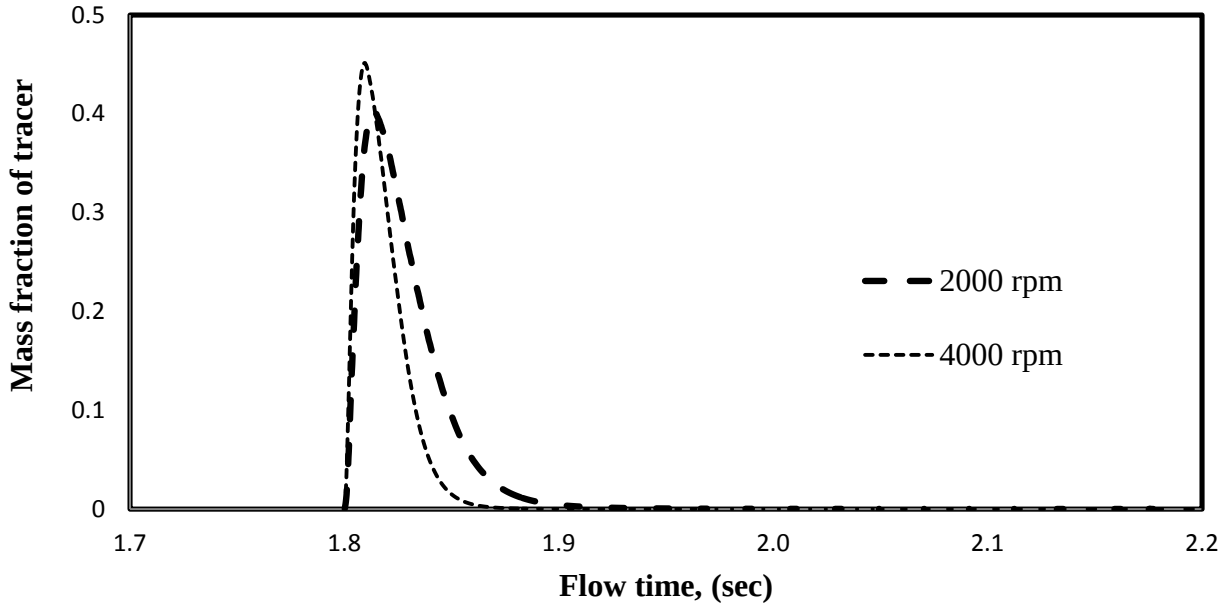

Fig.6.2 Comparison of mass fraction of tracer with respect to flow time at point 1 for square rotor-stator mixer

The variation of tracer concentration with time at point 2 and 3 is reported in Fig. 6.3. It can be concluded that at Points 2 and 3 mixing is similar and the mixing is only affected only by rotation speed. The required flow time is more at the 2000 rpm as compared to the 4000 rpm to gain a constant value. The required flow time to start the mixing process and to attain the uniformity in the square rotor-stator mixer is less at 4000 rpm.

As the Point 2 and Point 3 are in near to the stator holes jet so the time required to reaching the species to its maximum and minimum value is less than the Points 4-7, but more than the time taken at Point 1.

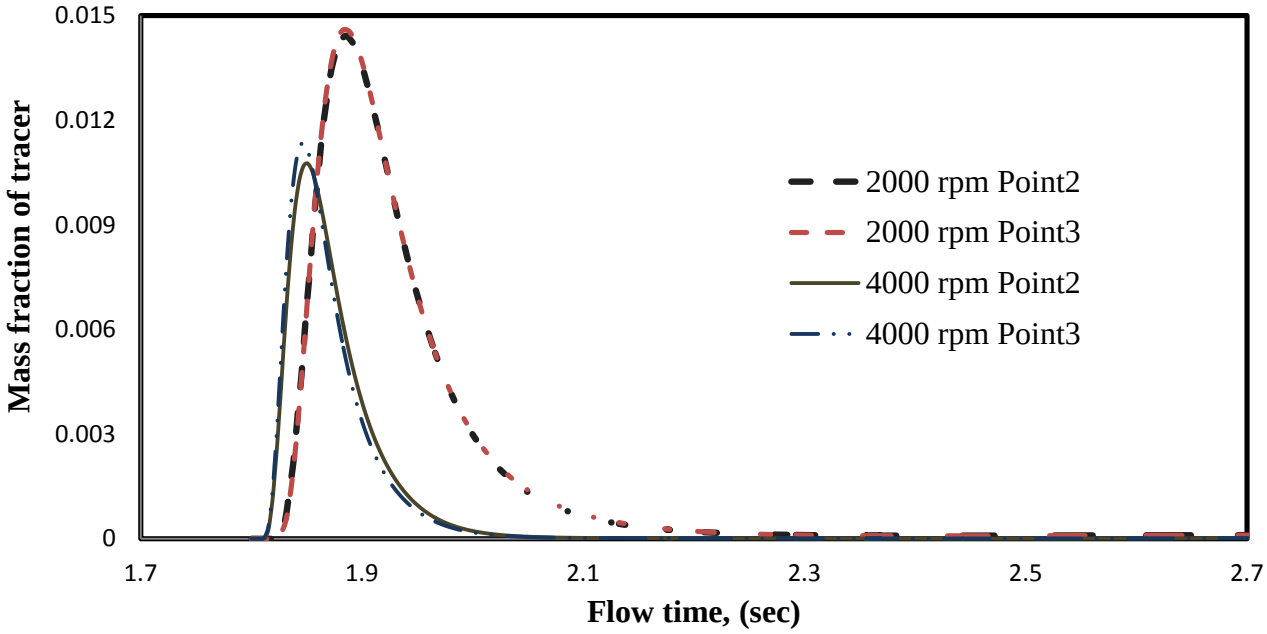

Fig. 6.3 Comparison of mass fraction of tracer with respect to flow time at point 2 and point 3 for square rotor-stator mixer

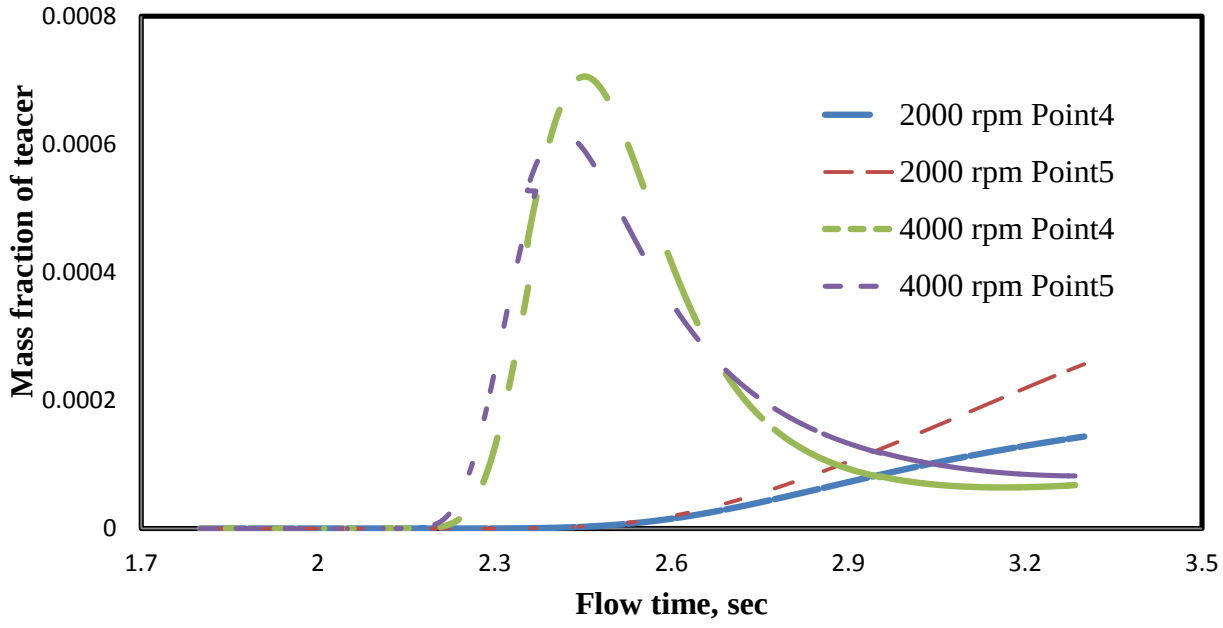

Fig. 6.4 Comparison of mass fraction of tracer with respect to flow time at point 4 and point 5 for square rotor-stator mixer

Fig. 6.4 shows that at an rpm of 2000 for both points 4 and 5 there is no mixing initiated before a flow time of 2.5 seconds and after that mass fraction goes up to 3.30. After that mass fraction continue to increase at point 5 and becomes constant at point 4. At an rpm of 4000 the scenario is completely different the mixing starts at a flow time of 2.2 and 2.16 for Point 4 and Point 5 respectively. The point of maxima is reached at Point 5 earlier than Point 4.

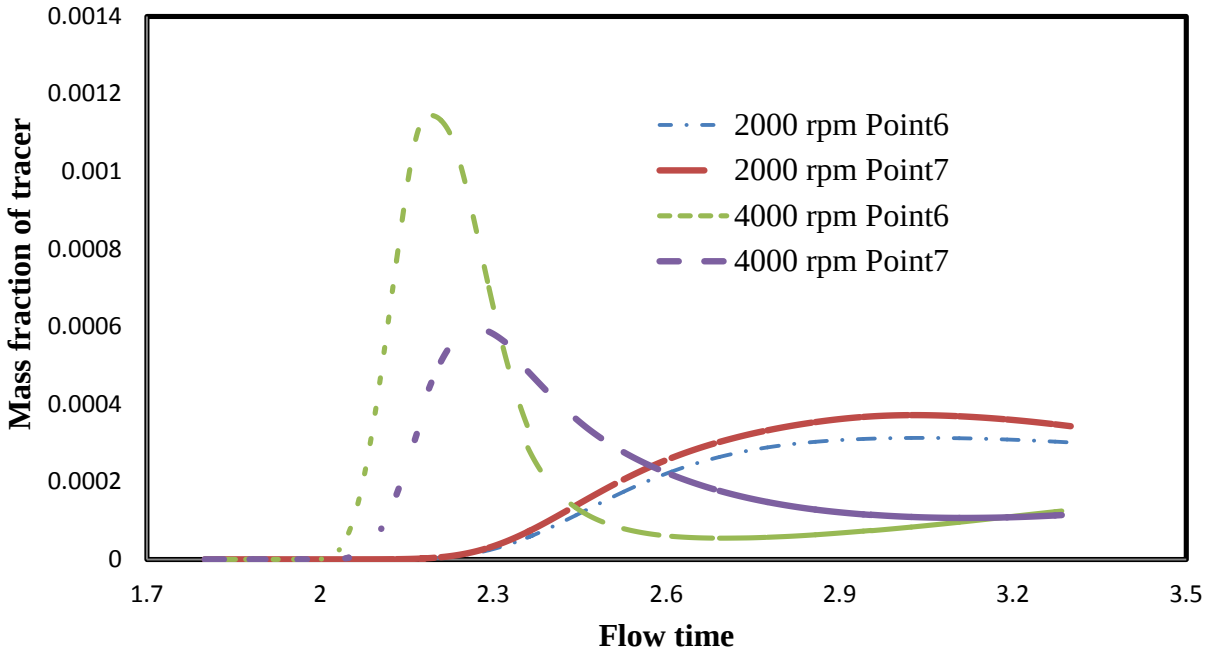

Fig. 6.5 Comparison of mass fraction of tracer with respect to flow time at point 6 and point 7 for square rotor-stator mixer

From Fig. 6.5 it can be seen that at 2000 rpm, the tracer reaches Point 6 at a flow time of 2.21 second and then increase. However after 3.3 second the tracer concentration starts declining. At Point 7 the tracer enters at 2.22 second and exit at 3.3 seconds. At an rpm of 4000 the tracer enters at Point6 at a flow time of 1.99 second and 2.05 second at Point 7. The maximum tracer concentration is attained at point 6 at 2.18 second followed by point 7 at 2.25 second. After reaching maxima both decline and then become constant.

6.2.2 Tracer concentration in proposed RSM

The tracer concentration at point 1 in the proposed novel mixer is shown in Fig. 6.6. At rotational speeds of 2000, 4000 and 6000 rpm tracer reaches point at 1.89 second and its concentration reaches maximum at 1.89 second. However tracer exis point 1 at 1.818 s, 1.811 s and 1.807 s at 2000, 4000 and 6000 rpm, respectively.

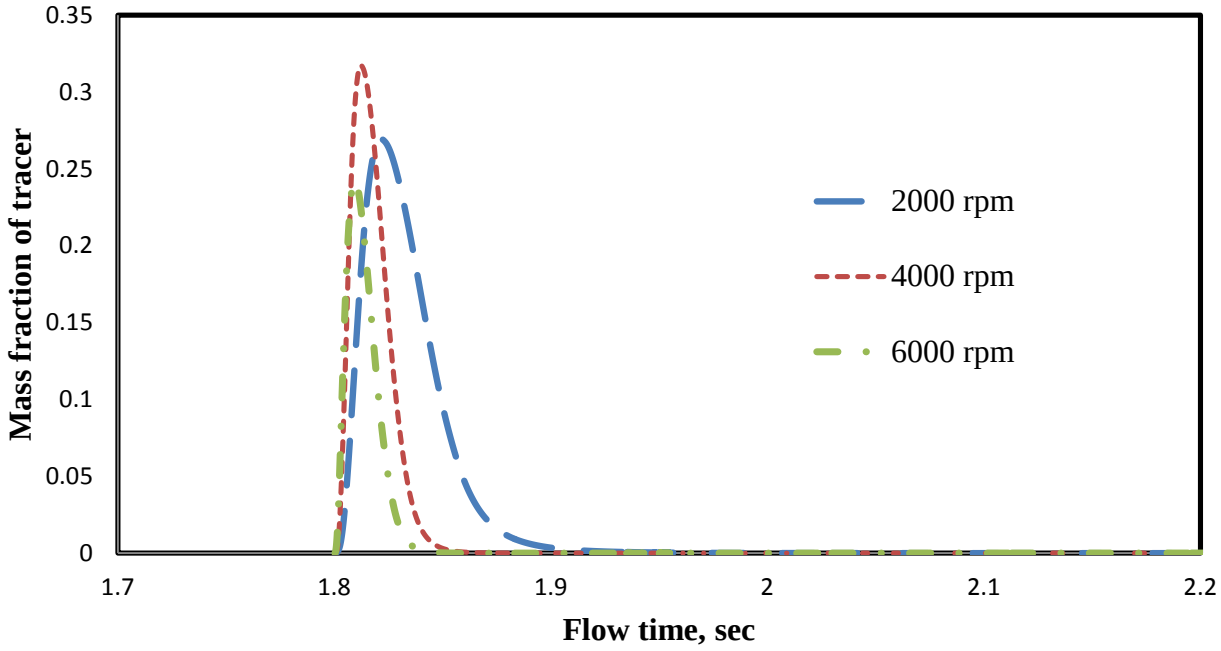

Fig. 6.6 Comparison of mass fraction of tracer with respect to flow time at point 1 for proposed novel mixer at different rotor speeds.

The tracer concentration at points 2 and 3, in the proposed novel mixer, is shown in Fig. 6.7. At a rpm of 2000 for both points 2 and 3 tracer enters at a flow time of 1.821 s, tracer concentration reaches maximum at 1.88 s and finally converges at 2.18 s. At an rpm of 4000 for both points 2 and 3, tracer enters at 1.8 s, tracer concentration reaches maximum at 1.84 seconds for point 2 and 1.83 for point 3, and finally converges at 1.97 and 1.95 seconds for point 2 and 3 respectively. At 6000 rpm for both points 2 and 3, tracer enters at 1.8 s reaches maximum at 1.84 s at point 2 and 1.822 at point 3, and finally converges at 1.94 seconds for both points.

Fig. 6.8 shows the variation in tracer concentration at points 4 and 5 at different rotor speeds. It can be seen tracer enters at 2.48 s and its concentration increases further. At an rpm of 4000 for both points 4 and 5 mixing starts at a flow time of 2.17 and 2.19 seconds respectively, tracer concentration reaches maximum at point at 2.5 seconds at point 4 and 2.41 s at point 5 and finally converges at 1.97 and 1.95 seconds for point 4 and 5 respectively.

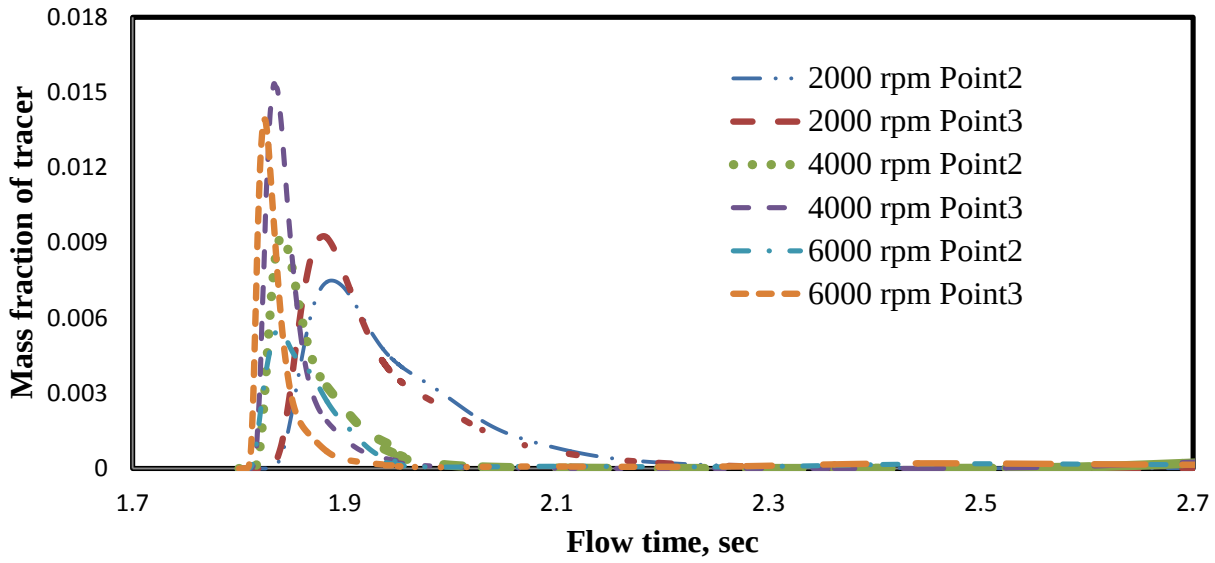

Fig. 6.7 Comparison of mass fraction of tracer with respect to flow time at point 2 and point 3 for proposed novel mixer

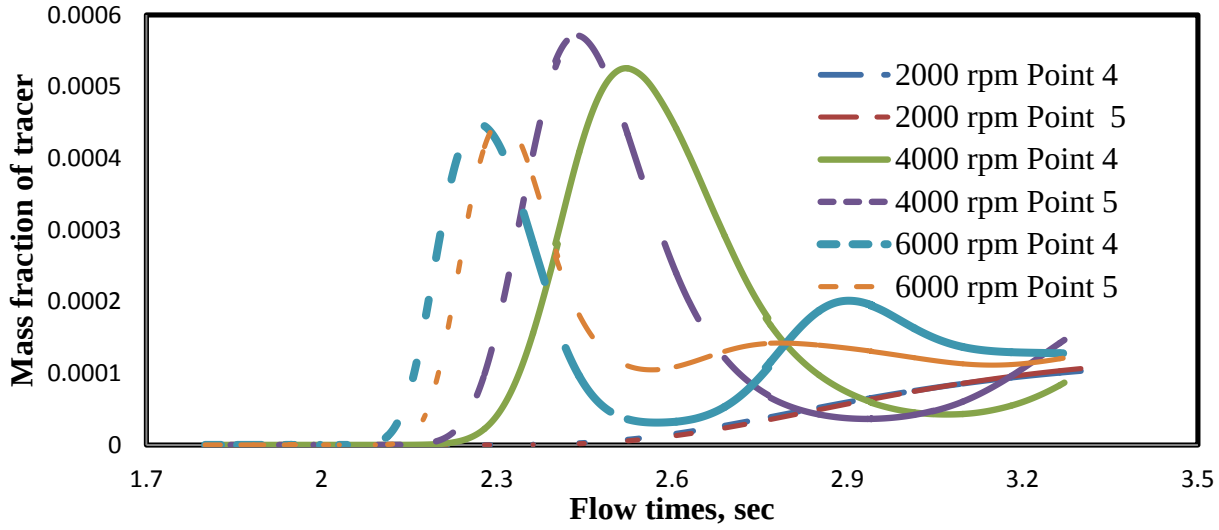

Fig. 6.8 Comparison of mass fraction of tracer with respect to flow time at point 4 and point 5 for proposed novel mixer

At 6000 rpm the tracer enters at smaller time as compared to 2000 and 4000 rpm. Tracer stays at points 4 and 5 for small times period and then its concentration decreases, and further starts increases after 2.6 s, and finally gets stable after 3.2 s. The fluctuating behavior at 4000 and 6000 rpm is because the proposed mixer is a batch type hence tracer has no exit so it is continuously present in the mixer and its mass fraction increases and decreases with time.

From Fig. 6.9 it can be seen that the tracer enters earlier at point 7 at 6000 rpm as compared to the 2000 and 4000 rpm. However at point 6, at 6000 rpm, the tracer enters at the same time as at rotor speed of 4000 rpm. For 2000 rpm the tracer is continuously increases at point 6 and 7 for the time span considered in the present work. Therefore it can be concluded that at higher rotor speed the mixing is faster and uniform as compared to the low rotor speed (≈ 2000 rpm). Further at higher rotor speed (≈ 4000 and 6000 rpm) the tracer concentration fluctuates and gets stable after 3.2 s.

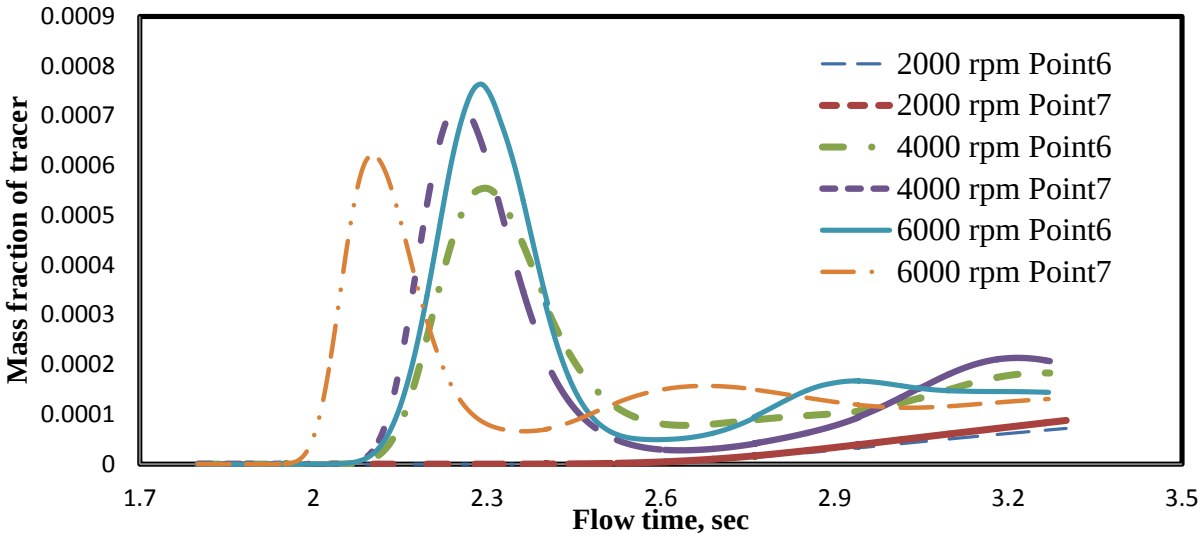

Fig. 6.9 Comparison of mass fraction of tracer with respect to flow time at point 6 and point 7 for proposed novel mixer

6.2.3 Tracer contours in the square holes and proposed RSM.

Fig 6.10 shows the distribution of tracer mass fraction in square holes rotor-stator mixer at 2000 and 4000 rpm. The contours for tracer mass fraction are drawn on a vertical plate at the center of

the mixer. It can be seen from the Fig. 6.10a that there exist dead zones in the region near the shaft and above the rotor-stator hence mixing is very poor in the same. The fluid in the tank is sucked by the region below the rotor stator and then it is passed upward by the rotor stator assembly through the square holes in the bulk. The region on the left and right side of the RSM shows the maximum mixing.

Figure 6.10b shows that at 4000 rpm the mixing has improved in the bulk region, however dead zone exist near the shaft. Due to the increase in rpm the fluid that flows from the rotor stator flows to a greater height hence though there is dead zone near shaft but the mixing has improved. The mixing has enhanced in the bottom bulk fluid region, i.e. below the rotor.

From Figure 6.11a it can be seen that even at 2000 rpm mixing is enhanced though there is dead zone near the shaft and in the corners of the mixer. This adequate mixing at low rpm is achieved due to the geometry of the proposed mixer. Since the above holes in the stator are slightly tilted towards upwards and below holes are tilted towards the bottom hence the fluid from the rotor stator assembly covers major part of the mixer. Figure 6.11b shows that there is uniformity in tracer distribution throughout in the bulk region of the proposed mixer at 4000 rpm. Though there is dead zone near the shaft but the tracer reaches the corners of the mixer. Fig. 6.11c shows that at 6000 rpm the dead zone vanishes keeping behind a very little zone that do not have tracer. Though the quantitative analysis of mixing enhancement has not carried out, however from the contours in Fig. 6.11c it can be concluded that the mixing at 6000 rpm in the proposed model is higher as compared to the 2000 and 4000 rpm. The mixing behavior in the existing square holes rotor-stator mixer and the proposed novel mixer has been analyses with the help of tracer pathlines at different rotor speeds (i.e. at 2000 rpm, 4000 rpm and 6000 rpm). Fig. 6.12 shows the tracer pathlines in the square holes rotor-stator at 2000 rpm: (a) front view, and (b) isometric. It can be concluded from Fig. 6.12 that the flow inside the tank is predominant in the axial direction. The tracer concentration is more in the bottom bulk fluid as compared to the top bulk fluid. The jets are in axial direction and the fluid moves more in the downward direction as compared to the upward direction. As the fluid strikes the wall its axial velocity gets zero then it moves in the downward direction. From Fig. 6.12 it can be seen that the tracer distribution is more in the bottom bulk region and also more uniform as compared to the top bulk fluid. There are more dead zones in this assembly as discussed earlier.

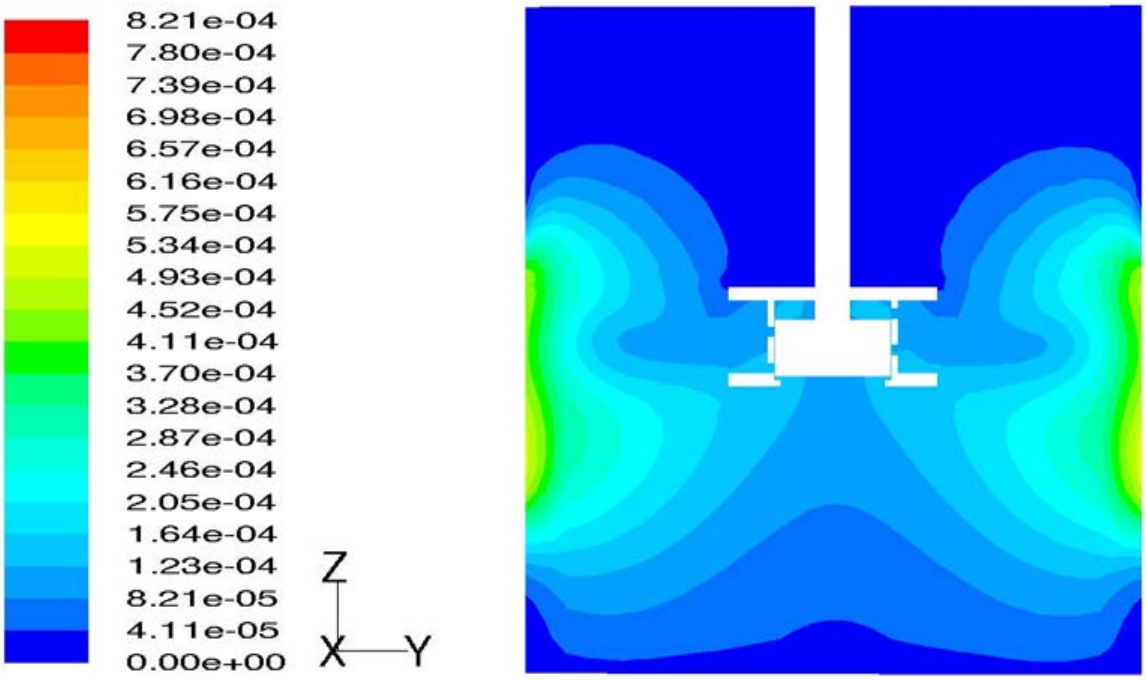

(a)

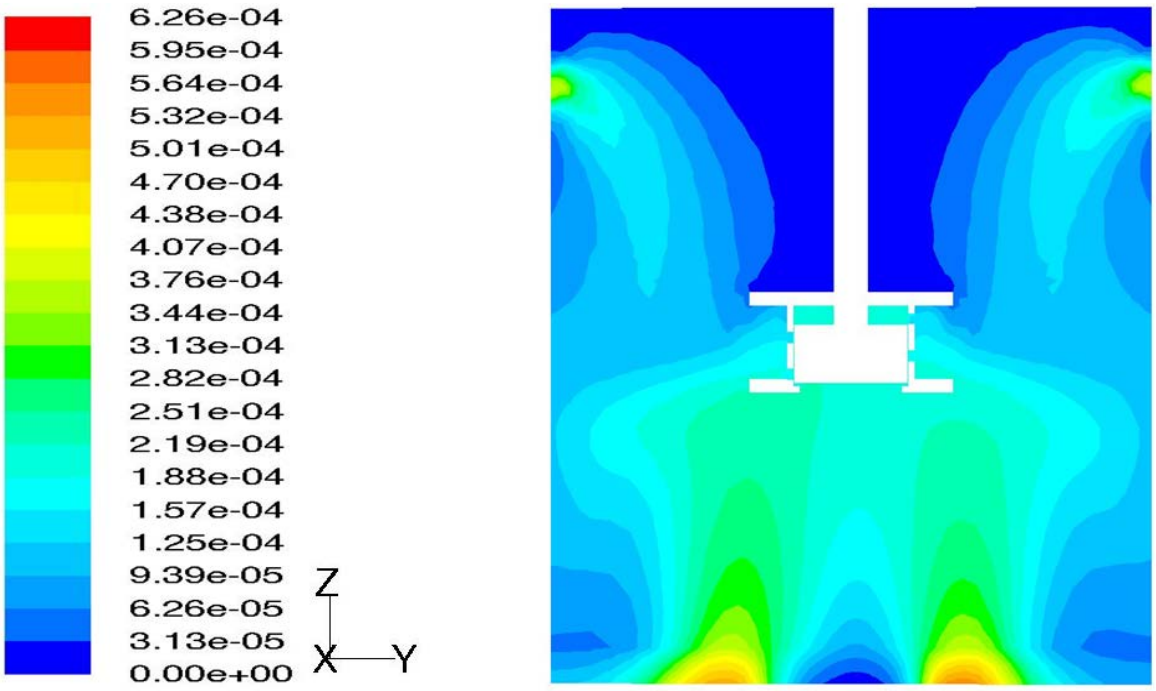

(b)

Fig. 6.10 Tracer distribution on a vertical plane in square holes rotor-stator mixer at (a) 2000 rpm, and (b) 4000 rpm

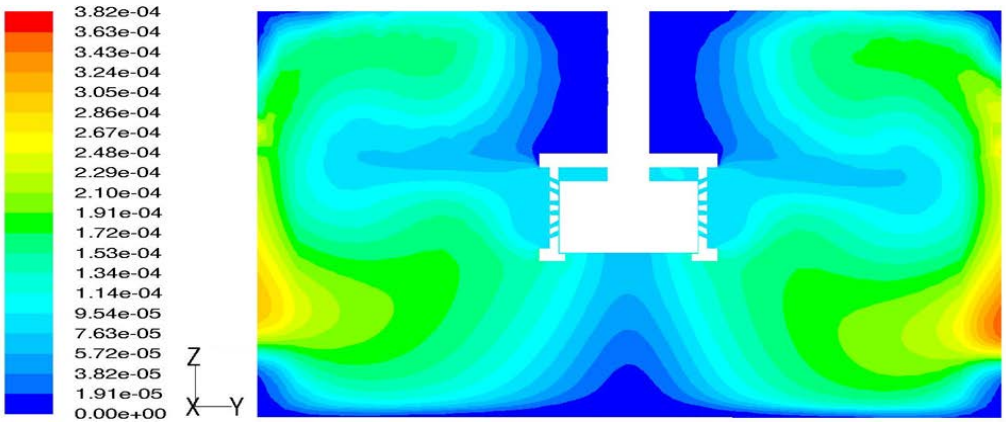

(a)

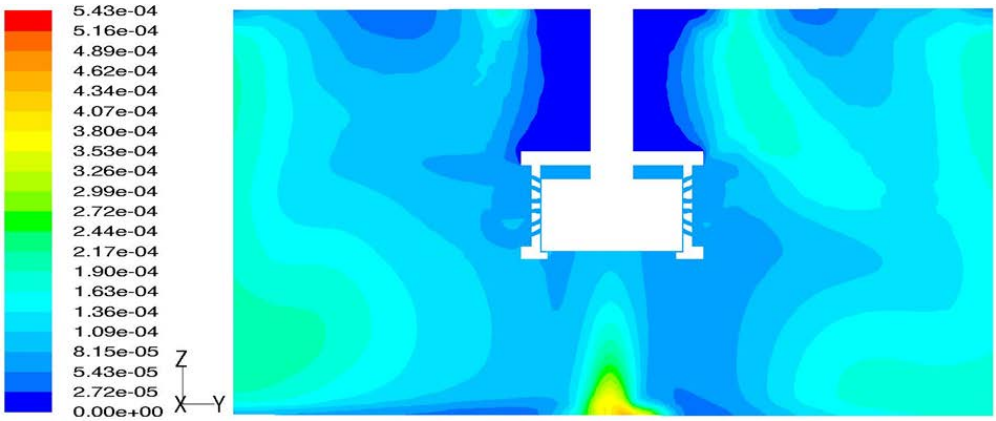

(b)

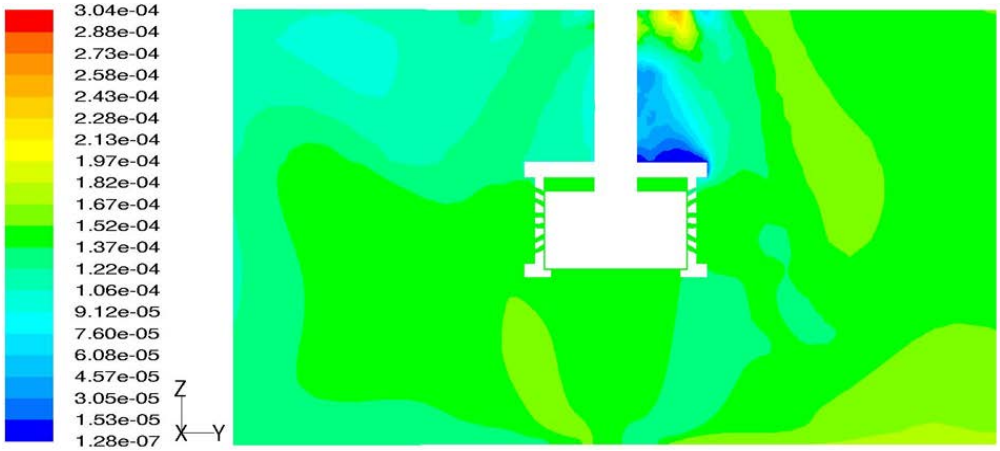

(c)

Fig. 6.11 Tracer distribution on a vertical plane in the proposed rotor-stator mixer at (a) 2000 rpm, (b) 4000 rpm, and (c) 6000 rpm.

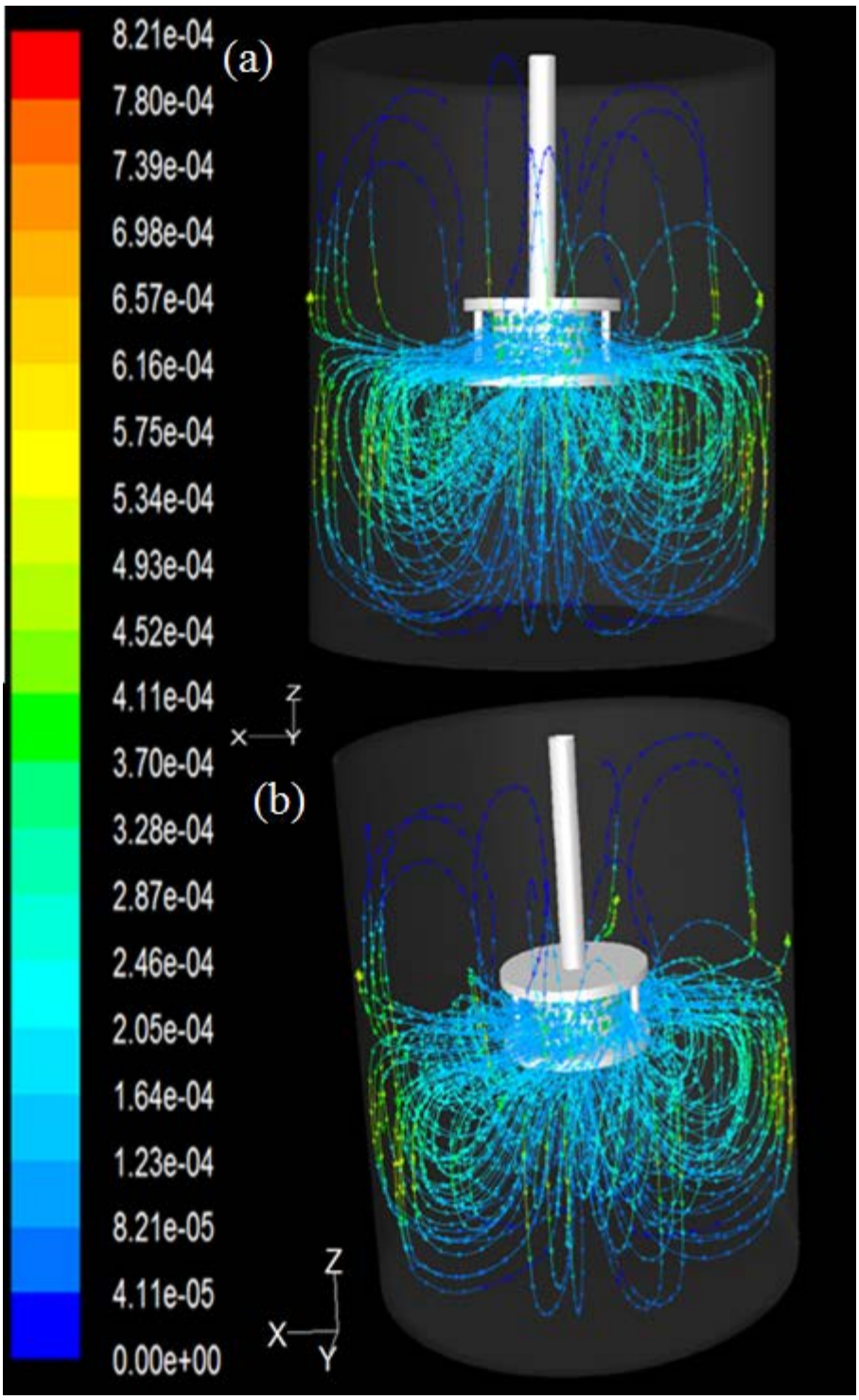

Fig. 6.12 Tracer pathlines in square rotor-stator mixer at 2000 rpm: (a) front view, and (b) isometric.

The tracer pathlines in the proposed mixer are shown in Fig. 6.13 at 2000 rpm. The direction of flow is changed in the proposed novel mixer from axial to radial direction. A circular motion in the fluid the stator was observed, which is generated because of the centrifugal force inside the tank. As the fluid passed the stator holes it start circulating in radial direction and the radial effect can be seen till the wall of the tank. However, there is no radial direction in the square holes mixer. The dead zones in this mixer are less as compared to the square holes mixer and there is more uniform mixing in this mixer. Mixing in the bottom bulk fluid is high in proposed novel mixer.

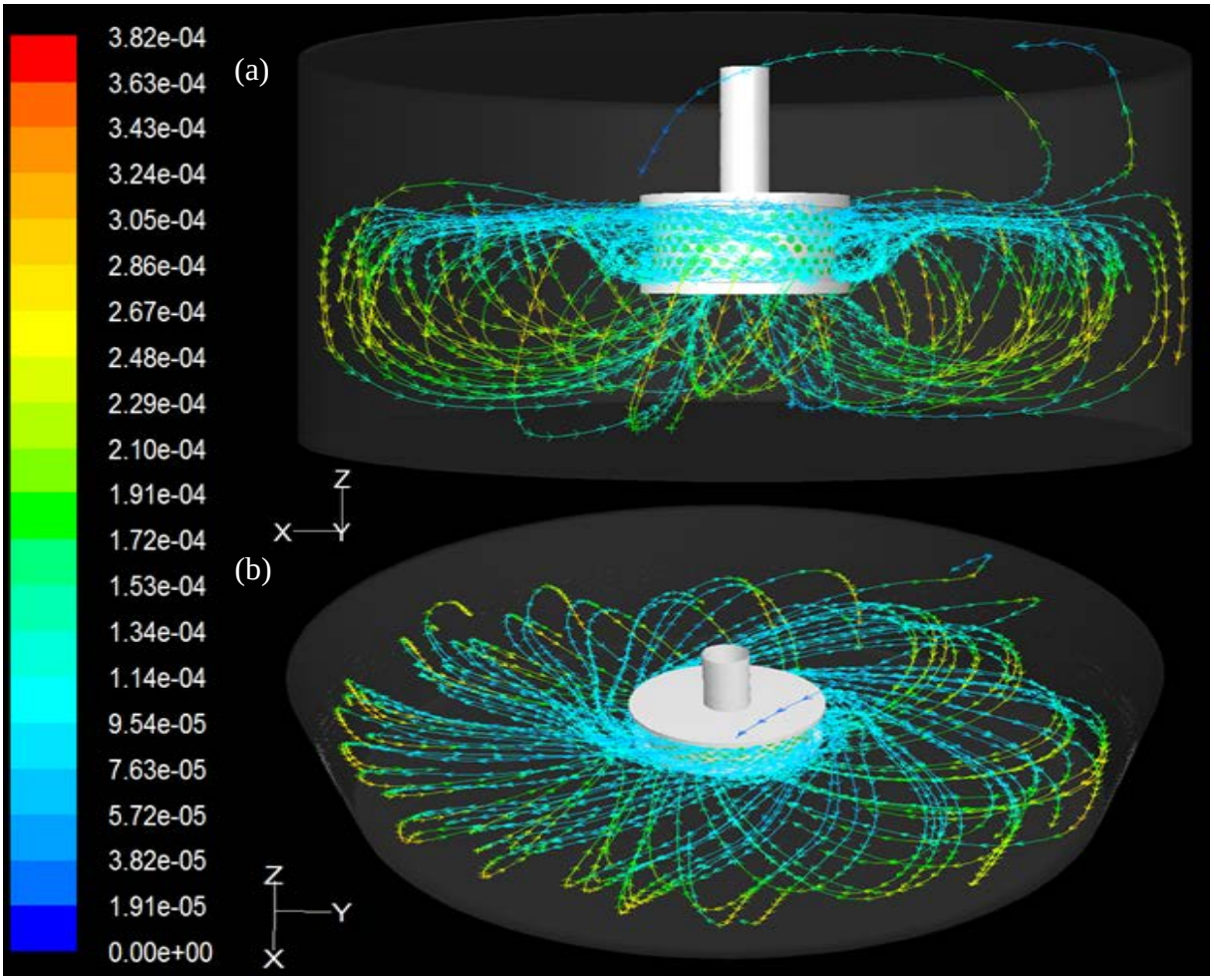

Fig. 6.13 Pathlines for the proposed novel mixer at the rotor speed of 2000 rpm: (a) front view, and (b) isometric view.

The uniformity in the tracer distribution is less in both the mixer at the lower rotor speed because the fluid is not able to reach to top bulk fluid. Therefore both mixers are simulated at 4000 rpm. The tracer pathlines at 4000 rpm are shown in Figs. 6.14–6.15, for square holes mixer and proposed mixer, respectively.

From Fig. 6.14 it can be observed that there is tracer is well distributed in the top bulk fluid but the path is same as in the axial direction. The jets of the fluid that comes from the square holes in upward direction are carried to a greater height because of higher rpm. As the jets moves in axial direction they fall on the tank walls and a more number of upward pathlines are observed as compared to that of 2000 rpm. The numbers of pathlines are more in the upward direction and hence the mixing is also high in the top bulk fluid as observed from the Fig. 6.14.

From Fig. 6.15, it can be observed that the flow fields are similar to that of 2000 rpm in the proposed mixer as discussed earlier. The radial direction is predominant over the axial direction, which is due to the centrifugal force generated in the tank. Top two layers of tilted holes will generate the disturbance in the top bulk fluid in the tank.

The radial direction is predominant over the axial direction and it is because of the centrifugal force generate in the tank. Top two layers of tilted holes will generate the disturbance in the top bulk fluid in the tank.

The tracer pathlines in proposed novel rotor-stator assembly are also reported at a rotor speed of 6000 rpm (Fig. 6.16). The flow behavior direction is similar to that of 2000 rpm and 4000 rpm in the proposed novel mixer but the mixing is more uniform higher rotor speed. From Fig. 6.16 it can be concluded that higher the rotor speed better the mixing and the dead zones also vanishes.

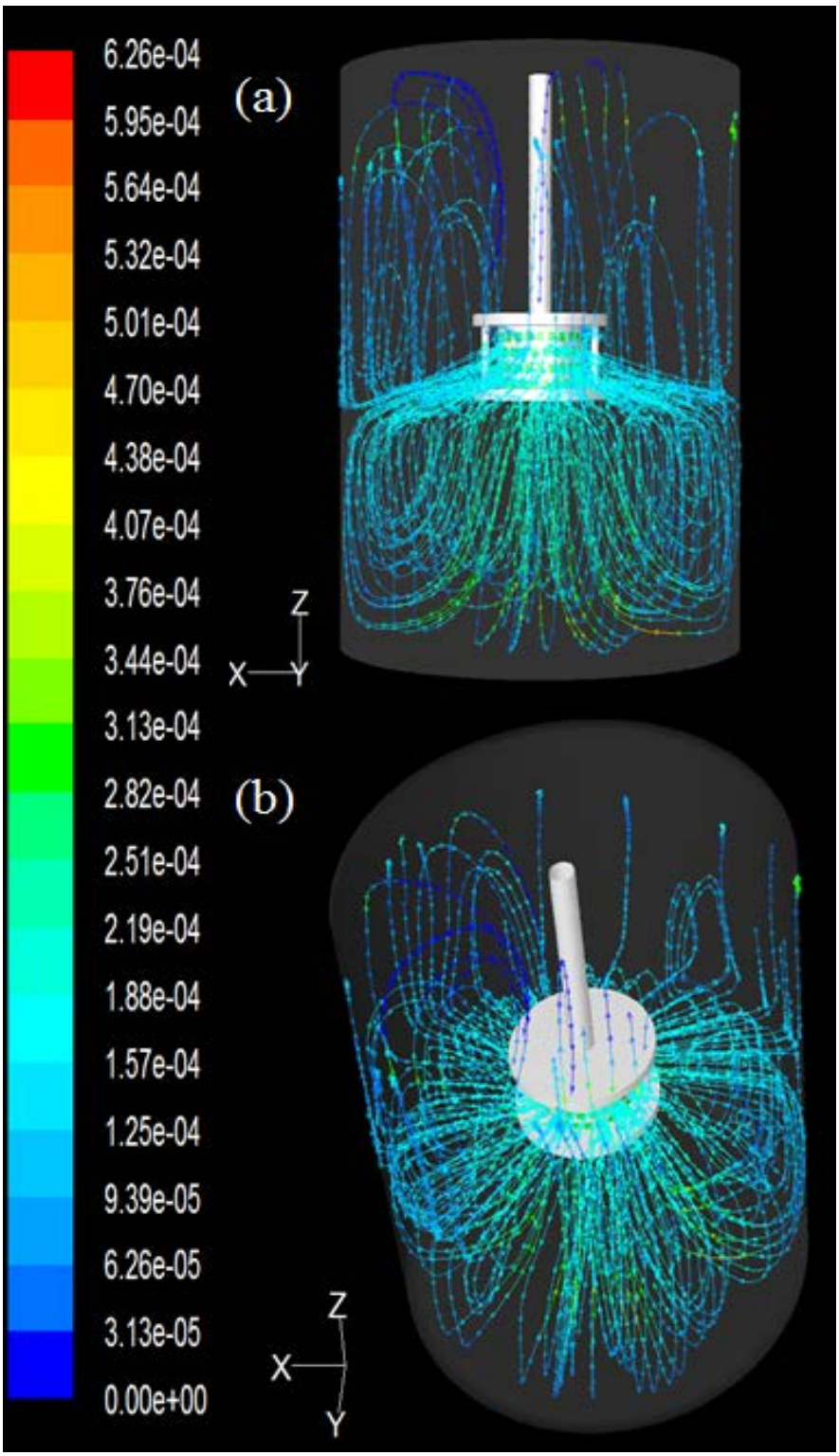

Fig. 6.14 Pathlines for the square rotor-stator mixer at 4000 rpm (a) front view, and (b) isometric view.

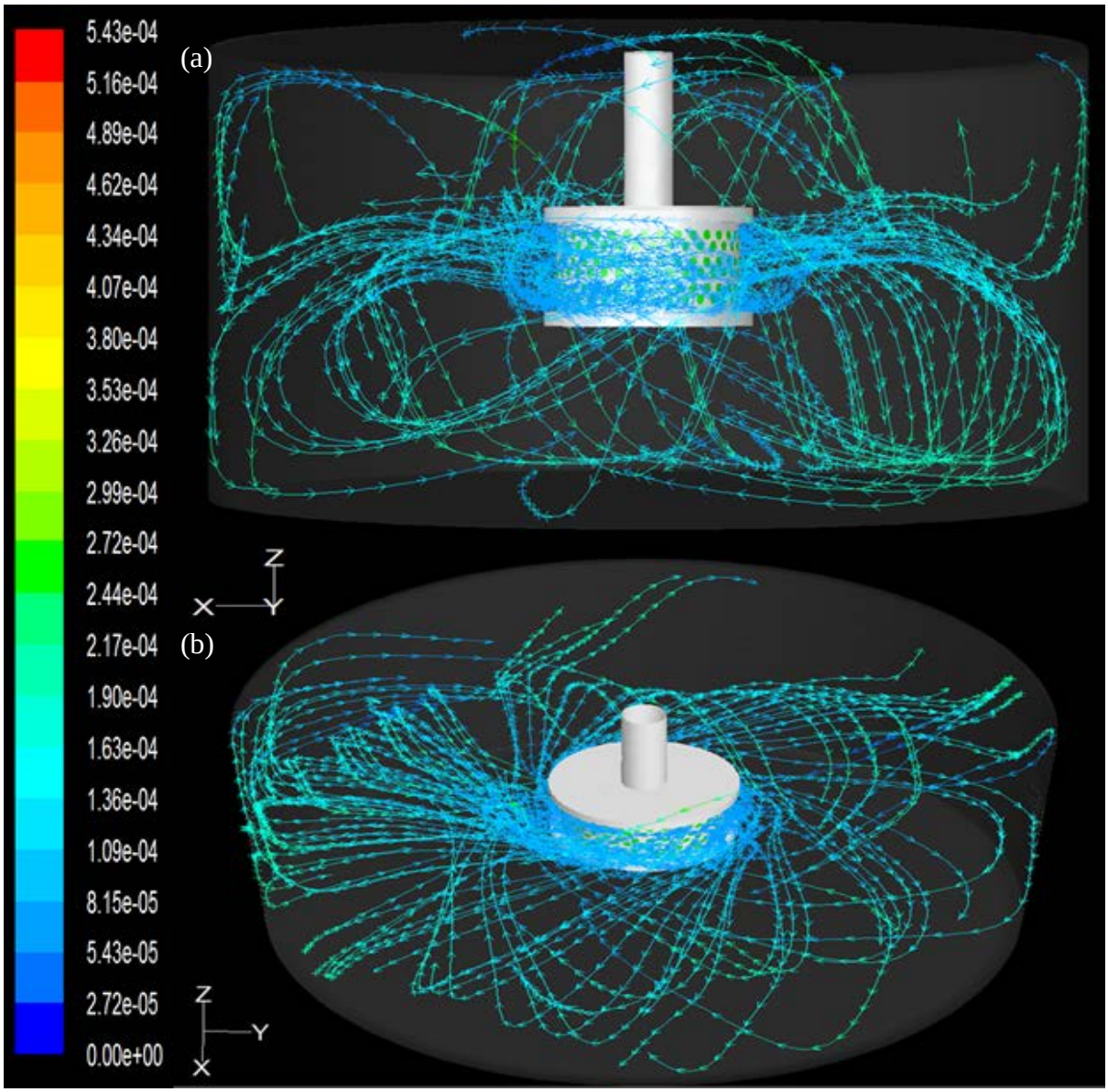

Fig. 6.15 Pathlines for the proposed novel mixer at 4000 rpm: (a) front view, and (b) isometric view.

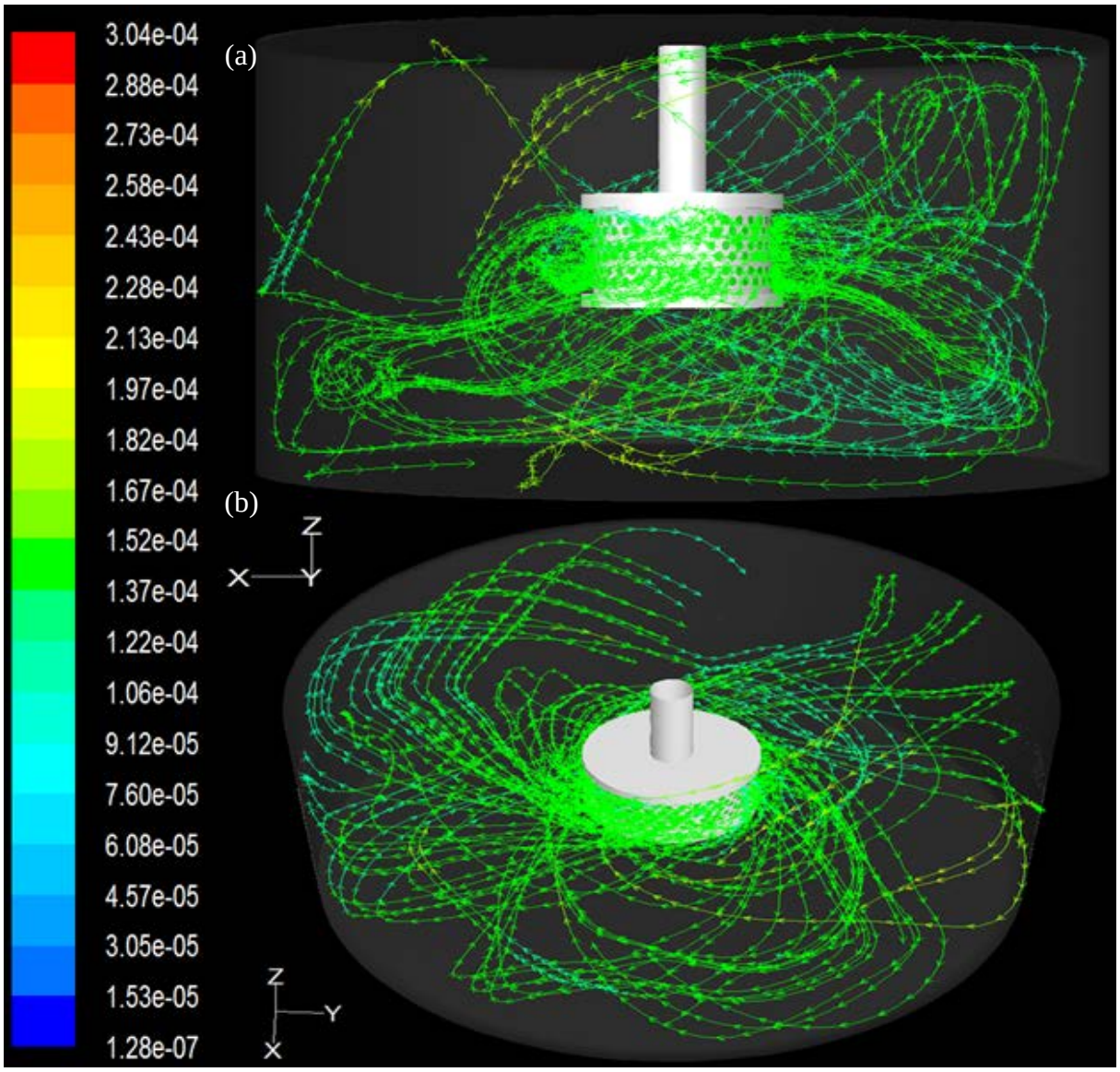

Fig. 6.16 Pathlines for the proposed novel mixer at 6000 rpm: (a) front view, and (b) isometric view.

CHAPTER 7

CONCLUSIONS AND RECOMMENDATIONS

In the present work the CFD modeling of an existing HSM and a proposed novel HSM design was carried out using k-ε turbulence model. The results in both existing and proposed design were reported in terms of power draw, flow patterns and energy dissipation. The simulations were carried out using transient sliding mesh with k-ε turbulence model at a rotor speed of 4000 rpm for the validation with the existing results. The existing HSM is comprised of square holes in the stator and a rotor with 4 blades and the proposed mixer design is comprised of tilted jets/holes in the stator, for the deep penetration in the mixing vessel.

The proposed novel mixer has been found good since the amount of power drawn for this mixer was less than the conventional square holes rotor stator mixer. Hence it can be concluded that the working and performance of a mixer is greatly affected by the shape and inclination of jets in the stator. Since in the proposed novel mixer the jets in the above region and in the below region were inclined in the positive and negative z direction respectively therefore the jets resulted in better mixing or in other words small dead zones. Also it was found that the dead zones generally occurred near the shaft and the corners of the existing mixer but were reduced in the proposed mixer greatly. The distribution of the tracer at a given point inside the mixer was greatly dependent on the location of a certain point in the mixer and also on the rpm of the rotor but when compared for the same rpm the distribution in case of proposed mixer was found to be better than the existing mixer. Though the maximum energy dissipation in any mixer occurs in the rotor swept region at different rpm but it was found more for the proposed mixer, other conditions being the same. The efficiency of the proposed mixer was also found in good agreement with the existing square holes rotor stator mixer. The mixing time required for the novel mixer was less than that of the existing mixer at a given rpm. Hence the novel mixer with the proposed geometry resulted in fast mixing at a less power.

Based on the present work it is further recommended to carry out simulations with horizontal circular stator holes and compare the results with the proposed RSM. Also it is proposed to carry out experiments for fluid hydrodynamics and mixing characteristics in the proposed RSM.

REFERENCES

Arratia, P.E., Lacombe, J.P., Shinbrot, T. and Muzzio, F.J., 2004. Segregated regions in continuous laminar stirred tank reactors, Chem Eng Sci, 59: 1481–1490.

Barailler F., Heniche M., Tanguy P.A., 2006. CFD analysis of a rotor-stator mixer with viscous fluids; Chemical Engineering Science 61, 2888 – 2894.

Brennan D.J. and Lehrer, I.H., 1976. Impeller mixing in vessels, experimental studies on the influence of some parameters and formulation of a general mixing time equation, Trans I ChemE, 54, 139–152.

Calabrese, R.V., Francis, M.K., Kevala, K.R., Mishra, V.P., Padron, G.A., Phongikaroon, S., 2002. Fluid dynamics and emulsification in high shear mixers. 3rd World Congress on Emulsions, Theme II, Conf.03, Lyon, France.

Doucet L., Ascanio G. And Tanguy P.A., 2005. Hydrodynamics characterization of rotor stator mixer with viscous fluids Chemical Engineering Research and Design, 83(A10), 1186–1195.

Elson, T.P., Cheesman, D.J. and Nienow, A.W., 1986. X-ray studies of cavern sizes and mixing performance with fluids possessing a yield stress, Chem Eng Sci, 41, 2555–2562.

Fang J.Z., Lee D.J., 2001. Micro mixing efficiency in static mixer. Chemical Engineering Science 56, 3797–3802.

Jasińska M., Bałdyga J., Cooke M., Kowalski A., 2013. Application of test reactions to study micromixing in the rotor-stator mixer (test reactions for rotor-stator mixer), Applied Thermal Engineering 57, 172–179.

Kowalski A.J., Cooke M., Hall S., 2011. Expression for turbulent power draws of an in-line Silverson high shear mixer. Chemical Engineering Science 66, 241–249.

Pacek A.M., Baker b., Utomo.A.T, 2007. Characterisation of Flow Pattern in a Rotor Stator High Shear Mixer" European Congress of Chemical Engineering (ECCE-6) Copenhagen, 16-20.

Solomon, J., Elson, T.P., Nienow, A.W. and Pace, G.W., 1981. Cavern sizes in agitated fluids with a yield stress, Chem Eng Commun, 11, 143–164.

Thakur R.K., Vial Ch., Nigam K.D.P., Nnauman E.B. and Djelveh G., 2003. Mixers in the Process industries: A Review; Institution of Chemical Engineers, Vol 81, 787–826.

Utomo A. T., Bakerb M., Pacek A. W., 2008. Flow pattern, periodicity and energy dissipation in a batch rotor–stator mixer, chemical engineering research and design 86, 1397–1409.

Utomo A., Bakerb M., Pacek A.W., 2009. The effect of stator geometry on the flow pattern andenergy dissipation rate in a rotor-stator mixer, chemical engineering research and design 87, 533–542.

Viazzo S., Sébastien P., Eric S., Randriamampianina A., Patrick B., 2012. High-order Large Eddy Simulations of Confined Rotor Stator Flows. Flow Turbulence Combust 88, 63–75.

Victor A.O., Kresta S.M., Paul E.L., 2004. Handbook of industrial mixing science and practice.

Zhang J., Xu S., Li W., 2012. High shear mixers: A review of typical applications and studies on power draw, flow pattern, energy dissipation and transfer properties. Chemical Engineering and Processing 57-58, 25-41.

Zhang Q., Yang C., Mao Z., and Junjuan M., 2012. Large eddy simulation of turbulent flow and mixing time in a gas-liquid stirred tank. Ind. Eng. Chem. Res 51, 10124–10131.